Applied Catalysis B: Environmental 240 (2019) 153–173

Contents lists available at ScienceDirect

Applied Catalysis B: Environmental

journal homepage: www.elsevier.com/locate/apcatb

Review

Megamerger in photocatalytic field: 2D g-C_3N_4 nanosheets serve as support of 0D nanomaterials for improving photocatalytic performance

Danlian Huang[a,b,*], Zhihao Li[a,b], Guangming Zeng[a,b,*], Chengyun Zhou[a,b], Wenjing Xue[a,b], Xiaomin Gong[a,b], Xuelei Yan[a,b], Sha Chen[a,b], Wenjun Wang[a,b], Min Cheng[a,b]

[a] College of Environmental Science and Engineering, Hunan University, Changsha, Hunan, 410082, PR China
[b] Key Laboratory of Environmental Biology and Pollution Control (Hunan University), Ministry of Education, Changsha, Hunan, 410082, PR China

ARTICLE INFO

Keywords:
g-C_3N_4 nanosheets
Carbon nanodots
Noble metal atoms
Semiconductor nanoparticles
0D/2D nanostructure

ABSTRACT

Over the past years, two dimensional (2D) graphitic carbon nitride nanosheets (CNNs) have attained increasing interest in the study of graphitic carbon nitride (g-C_3N_4) due to their superior physical-optical properties as photocatalyst. More and more researchers attempt to design photocatalytic systems based on CNNs to realize the control of photocatalyst morphology for enhancing performance. Hence their combination with zero dimensional (0D) nanomaterials, which frequently serve as guest materials, has witnessed great progress. Therefore this review introduces the latest fabrication strategies of CNNs based on conventional strategies and firstly summarizes their photocatalytic properties systematically. More important, typical advanced examples combining CNNs with 0D nanomaterials like carbon nanodots, noble metal atoms and semiconductor nanoparticles are presented for their characteristic 0D/2D nanostructures, which have never been reported in any previous reviews up to now. Their preparation, photocatalytic mechanisms and performance influence factors are deeply discussed. In addition, three kinds of multicomponent complex systems, which take advantages of 0D nanomaterials/CNNs ingeniously, are elaborated on their charge-transfer pathways in our review. Finally, the current challenges and development ideas of 0D nanomaterials/CNNs systems in photocatalytic applications are proposed. This review enriches the knowledge in the applications of CNNs and paves road to the combination of 0D materials with CNNs and even other 2D materials.

1. Introduction

With the rapid growth of modern industrialization and population, environmental pollution and energy crisis are becoming more and more serious global threats to the sustainable development of human society [1–5]. So the utilization of solar energy is being explored constantly for its environmentally friendly and inexhaustible characters [6–8]. As a new strategy to take advantages of solar energy, semiconductor photocatalysis technology is becoming a focus of scientific research for its green and energy-efficient characteristics compared to biologic and chemical methods [9–13]. Since Fujishima and Honda successfully used TiO_2 as photoanode for water splitting in 1972 [14], an increasing number of semiconductor materials, such as boron nitride [15], black phosphorus [16], ZnO [17], Bi_2WO_6 [18], have been explored in photocatalytic field. And besides hydrogen production [19,20], their applications are expanded to organic pollutants degradation [21–23], carbon dioxide reduction [24,25], disinfection [26] and so on.

Among these materials, graphitic carbon nitride (g-C_3N_4) has become the new pet for its distinctive optical properties since the pioneering photocatalytic studies of g-C_3N_4 for water splitting under visible light [27]. Polymeric g-C_3N_4 is non-metallic and non-toxic, shows high stability in acidic/basic environment and can be easily prepared by readily available precursors, which make it have more realistic significance to put g-C_3N_4 into the applications of photocatalysis [28]. However, g-C_3N_4 prepared by conventional methods without further treatment is composed of numerous layers of two-dimensional (2D) counterparts, which is called bulk g-C_3N_4 (BCN) [29]. BCN possesses a low specific surface area and irregular morphology that attenuate the electron transfer in the material and limit its photocatalytic performance to a great extent [30].

Therefore, strenuous efforts have been made to improve the photocatalytic performance of BCN like heteroatoms doping [31], nanostructure design [32], heterojunction construction [33], etc. One way is to fabricate different dimensional g-C_3N_4 like zero-dimensional (0D) g-C_3N_4 quantum dots (QDs) [34], one-dimensional (1D) g-C_3N_4 nanotube/nanofiber/nanorod/nanowire [35–38], 2D g-C_3N_4 nanosheets

* Corresponding authors at: College of Environmental Science and Engineering, Hunan University, Changsha, Hunan, 410082, PR China.
E-mail addresses: huangdanlian@hnu.edu.cn (D. Huang), zgming@hnu.edu.cn (G. Zeng).

https://doi.org/10.1016/j.apcatb.2018.08.071
Received 12 May 2018; Received in revised form 2 August 2018; Accepted 28 August 2018
Available online 31 August 2018
0926-3373/

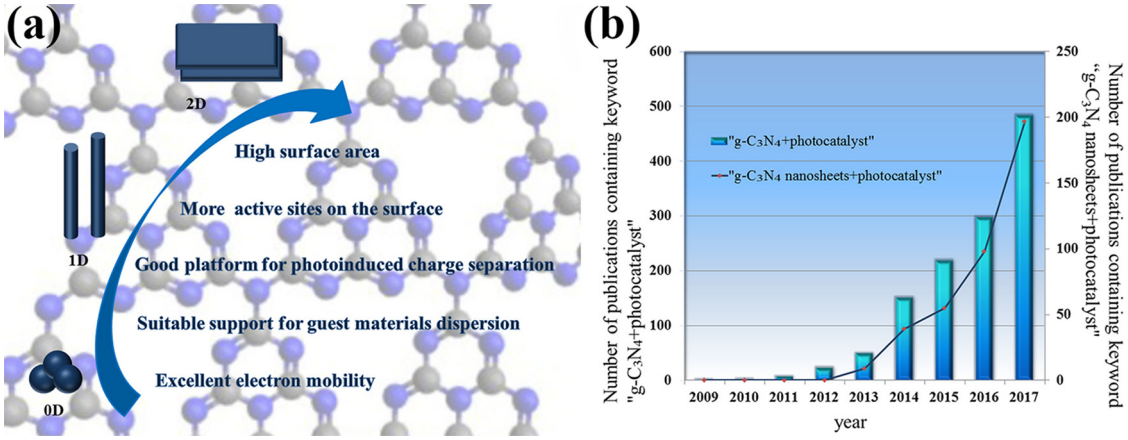

Fig. 1. (a) The advantages of 2D CNNs in comparison with 0D and 1D g-C_3N_4. **(b)** Evolution of the number of publications concerning the keywords "g-C_3N_4 + photocatalyst" and "g-C_3N_4 nanosheets + photocatalyst" on indexed journals between 2009 and 2017. The data comes from the research on "Web of Science".

(CNNs) [39], three-dimensional (3D) g-C_3N_4 sphere/hollow sphere [40,41]. Especially, 2D CNNs attract more attention due to their high surface areas, more active sites on the surface, excellent electron mobility, ability to serve as suitable support for guest materials dispersion and good platform for charge carrier separation (Fig. 1a).

In the past years, many studies have been conducted on CNNs since their successful fabrication by Niu et al. [42]. Papers on indexed journals concerning the keywords "g-C_3N_4 nanosheets + photocatalyst" increase year by year and they accounts for approximately two-fifth of all "g-C_3N_4 + photocatalyst" in 2017 (Fig. 1b). Many excellent reviews have been published on the applications of g-C_3N_4 in the photocatalytic field [43,44]. However, few reviews are written for CNNs specially. Zhang et al. overviewed the two synthetic strategies of CNNs and their functionalization and applications in various fields besides photocatalysis with a broad view in 2015 for the first time [45]. And Dong et al. emphasized on the comparison of various exfoliation approaches to BCN and briefly introduced the photocatalytic applications of CNNs in the same year [46]. The most recent review by Ding et al. presented the preparation of different dimensional g-C_3N_4 and their combination with other photocatalyst systematically [47]. But the content of 2D CNNs was not specific and their superiority was not emphasized. So urgent work needs to be done to summarize the latest progress of CNNs.

At the same time, with the detailed study on photocatalytic materials structure over the past few decades, the fabrication of photocatalyst is no longer just finished through the direct combination of different materials. There is a developing trend that more and more efforts are put on the micromorphology controlling of material to consummate its physical characters and realize perfect combination for enhanced photoactivity [48–52]. As a kind of newly emerging semiconductor materials, CNNs can serve as an outstanding substrate when combining with other materials, which greatly facilitate to control the morphology of the designed photocatalyst and improve the photocatalytic performance. Hence, many strategies have been taken to load different materials onto the surface of CNNs for enhancing activity in recent years [53–56]. Among them, 0D nanomaterials attract quite a lot interest to combine with CNNs as guest materials due to their high specific surface areas, short charger-transfer length, easily controllable size and distribution. For example, carbon nanodots can serve as electrons (e^-) sink to promote the separation of electron-hole pairs in the systems [57], noble metal atoms can enhance the absorption ability of light [58], semiconductor nanoparticles (NPs) can form heterojunction with CNNs [59]. At the same time, CNNs show a perfect match in their combination with 0D nanomaterials. First, they serve as support and can confine the growth or aggregation of 0D nanomaterials for the N-binding and cavities on their surface, which contribute to smaller size and better distribution of 0D nanomaterials [60–62]. Second, the 2D morphology maintain the stability of CNNs compared to 0D/1D morphology and endows them with large surface area for better light absorption and pollutants adsorption ability, which greatly promote the photocatalytic efficiency of the systems. Third, the reduced thickness of CNNs can accelerate the charge carrier transition between them and 0D nanomaterials [63]. Therefore, many 0D/2D structural photocatalysts combining CNNs with 0D nanomaterials were designed in the past years and they exhibited excellent performance in the photocatalytic applications.

Thus, the main purpose of this review is to summarize the latest progress in the combination of CNNs with 0D nanomaterials to fabricate new photocatalyst with excellent performance. We first introduce the conventional strategies and some improved methods for CNNs preparation and the photocatalytic properties of them briefly. Then we present the latest study on the decoration of CNNs with several 0D nanomaterials including carbon nanodots, metal atoms and semiconductor nanoparticles. At the same time, the fabrication, photocatalytic mechanisms and performance influence factors of these 0D nanomaterials/CNNs systems are discussed specifically. Subsequently, more complex systems based on 0D nanomaterials/CNNs are generally classified. Typical examples are presented and the charge-transfer pathways of these systems during photocatalytic process are illustrated. Finally, we summarize the challenges need to be focused on and forecast the future of CNNs in the photocatalytic field. From this review, the readers will learn about the superiority of CNNs in the design of photocatalytic system and understand the charge carrier transition mechanisms and performance influence factors in 0D/2D nanostructural photocatalyst. We hope this review can give readers some inspiration and furtherly promote the development of CNNs applications.

2. CNNs as host materials for photocatalysis

2.1. Fabrication strategies of CNNs

g-C_3N_4 can be typically prepared by the polycondensation of nitrogen-rich organic precursors such as melamine [64], cyanamide [65], dicyandiamide [66], urea [67], thiourea [68], guanidine hydrochloride [69] and so on (Fig. 2a). But without further treatment, these obtained 3D BCN with numerous layers of 2D counterparts exhibit moderate performance in the photocatalytic applications. So some strategies preparing CNNs have been explored in the past years.

Two conventional strategies for the fabrication of CNNs have been summarized by Zhang et al. systematically [45], which include top-down strategy that prepares CNNs by destroying the weak van der Waals forces between the C–N layers of BCN and bottom-up strategy that assembles the building molecules in a 2D manner (Fig. 2b). In the

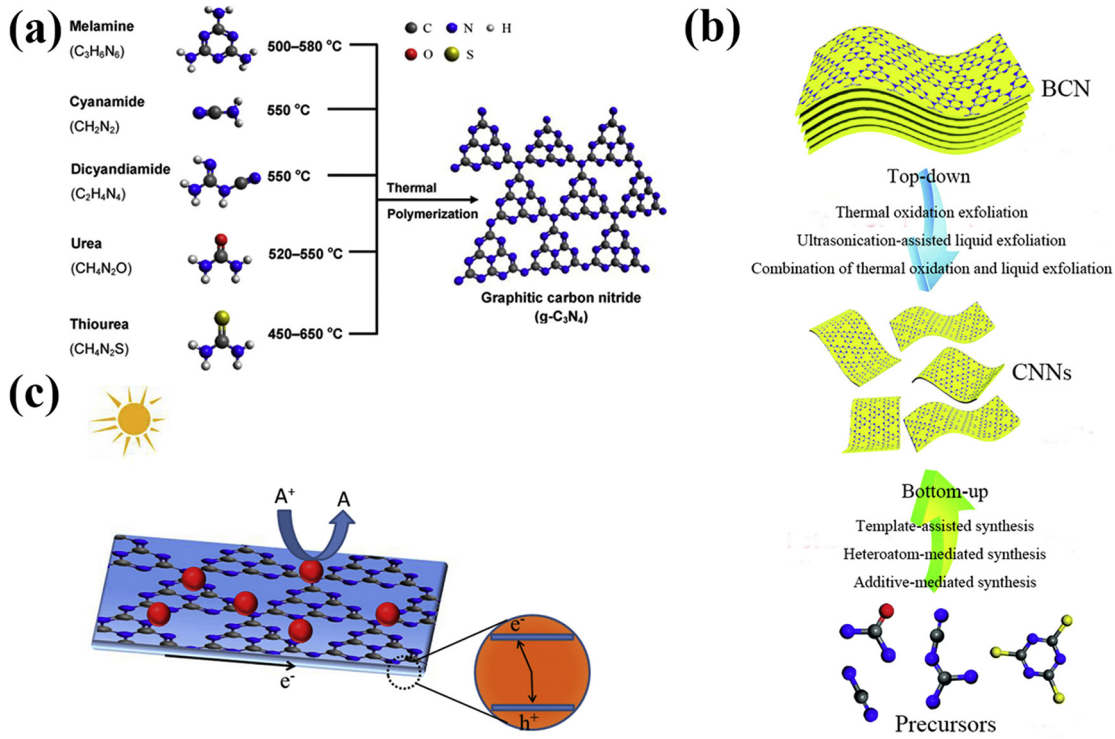

Fig. 2. (a) The synthesis process of g-C_3N_4 by thermal polymerization of different precursors such as melamine, cyanamide, dicyanamide, urea and thiourea. Reprinted with permission from Ref. [61]. Copyright 2016 American Chemical Society. **(b)** The top-down and bottom-up fabrication strategies for CNNs. **(c)** The charge transfer of CNNs during the photocatalytic process under visible light. Reprinted with permission from Ref. [45]. Copyright 2015 Royal Society of Chemistry.

top-down strategy, three main synthetic approaches can be adopted to exfoliate BCN including thermal oxidation exfoliation [70], ultrasonication-assisted liquid exfoliation [71] and combination of thermal oxidation and liquid exfoliation [72]. This strategy is a facile and easily controlled method to prepare CNNs but its low-yield and time-consuming characters limit its applications. In the bottom-up strategy, there are three main methods including template-assisted synthesis [73], heteroatom-mediated synthesis [74] and additive-mediated synthesis [75]. It is a scalable synthetic strategy and has advantages for the mass production of CNNs but followed a more complex process.

Based on the conventional strategies, more efficient methods have been developed to prepare CNNs in recent years. One way is promoting the exfoliation efficiency of BCN. For example, Bu et al. exfoliated BCN through wet mechanical grinding method and the yield of CNNs reached 90% [76]. Qiu et al. prepared CNNs by calcining BCN under H_2 atmosphere, which used the reaction of H_2 with C and N species in CNNs to prevent their re-stacking [77,78]. And the yield was much higher than that of those calcined in air. Yang et al. introduced hydrochloric acid during the liquid-exfoliation and hydrothermal treatment of urea-derived BCN [39]. The protons produced by hydrochloric acid intercalated into the layered structure of BCN and attached to strand nitrogen atoms, which contributed to efficient delamination of BCN [79]. The other way is pretreating the organic precursor to promote the formation of CNNs instead of BCN during the synthetic process. For example, Hong et al. pretreated melamine hydrothermally under 200 °C before being calcined [80]. And they obtained high-performance CNNs with 3 nm thickness successfully. They also found that the introduction of hydrochloric acid during the hydrothermal treatment on melamine could realize to control the thickness and performance of CNNs [30]. Liu et al. firstly treated dicyandiamide by the hydrothermal process and then heated it with microwave to fabricate CNNs [81]. The hydrothermal pretreatment contributed to form the melamine-cyanurate complex, which facilitated the generation of porous CNNs under the microwave-assisted thermolysis.

In conclusion, exfoliation of BCN is a frequently used method to prepare CNNs at present. Also, pretreating the precursors to prepare CNNs has been explored constantly. The fabrication of CNNs is becoming more and more efficient by these strategies, which facilitates their applications in photocatalytic field. What's more, studies realize the control on thickness of CNNs during preparation process. This contributes to the fabrication of CNNs with different physical characteristics and shows the adjustment of CNNs in the photocatalyst synthesis for different needs.

2.2. Photocatalytic properties of CNNs

g-C_3N_4 has a moderate band gap of 2.7 eV, which corresponds to an optical wavelength of 460 nm. This optical wavelength matches well with the visible spectral range of sunlight and makes g-C_3N_4 a promising photocatalyst [82]. Besides, from a thermodynamics perspective, the positions of the valence band (VB) and conduction band (CB) of a semiconductor, which determine the reduction and oxidation power of photogenerated carriers, are also important for the process of artificial photoredox reactions. As for g-C_3N_4, it has a CB level of −1.3 eV (vs. NHE at pH 7) and VB level of + 1.4 eV (vs. NHE at pH 7) [83], which make it satisfy the most mainstream photocatalytic reaction like water splitting [84], CO_2 reduction [85], organic pollutants degradation [86] and so on. The standard redox potentials of the reactions are shown in Table 1.

As a constituent part of BCN, CNNs exhibit a similar layered feature to graphene. Their hundreds of nanometers in length and width as a platform show exceptional advantages for the deposition of various compounds with different sizes and form effective heterointerfaces for charge transfer [87,88]. And better than graphene with zero-bandgap character, CNNs is a typical polymeric semiconductor with an sp^2 π-conjugated system, which facilitates their applications in the fabrication of nanosheets-based photocatalyst [45]. What's more, due to the ultrathin 2D nanostructure, the photocatalytic activity of CNNs is enhanced for the improvement in light absorption, charge carrier separation and increased specific surface area compared to BCN (< 10

Table 1
The standard redox potentials for the common reaction in phtocatalytic field.

Reaction	E°(V) vs NHE at pH 0
$2H^+ + 2e^- \rightarrow H_2$ (g)	0
O_2(g) + $e^- \rightarrow O_2^-$(aq)	−0.33
CO_2(g) + $2H^+ + 2e^- \rightarrow$ CO(g) + H_2O	−0.11
CO_2(g) + $6H^+ + 6e^- \rightarrow CH_3OH$(aq) + H_2O	+0.03
CO_2(g) + $8H^+ + 8e^- \rightarrow CH_4$ (g) + H_2O	+0.17
$2CO_2$(g) + $9H_2O + 12e^- \rightarrow C_2H_5OH$(aq) + $12OH^-$	+0.07
$2H_2O$(aq) + $4h^+ \rightarrow O_2$(g) + $4H^+$	+1.23
O_2(g) + $2H^+ + 2e^- \rightarrow H_2O_2$(aq)	+0.70
H_2O_2(aq) + $2H^+ + 2e^- \rightarrow 2H_2O$	+1.78
$OH^- + h^+ \rightarrow$ ·OH	+2.69

$m^2 g^{-1}$) [89]. At the same time, the thickness or, in other words, the layer number of 2D nanomaterials, influences the electronic structures of them in a large part. When the thickness is reduced, the wave propagation in 2D crystals will be confined and their bandgap will become larger due to the shift of CB and VB in opposite directions and the changed photophysical behavior of charge caused by quantum confinement [42]. So CNNs usually possess larger band gap than BCN and CNNs with different thickness exhibit discrepant performance. For example, Zhang et al. reported that the bilayered CNNs had much better visible light adsorption than the single-layered CNN for its unique electronic structure [90]. Tong et al. prepared ultrathin CNNs with seven-atomic thickness through the liquid exfoliation of BCN, which promoted the charge migration and separation efficiency by 2 times more than BCN [91]. CNNs with different thickness prepared by Hong et al. through hydrochloric acid-induced hydrothermal assembly approach exhibited higher H_2 evolution with the decrease of their thickness [30]. Therefore, controlling the thickness of CNNs is a suitable strategy to improve the performance of photocatalytic system based on them.

To summarize recent studies on CNNs, the delamination of BCN into CNNs induces unique physicochemical properties as follows: First, compared to BCN, CNNs endow g-C_3N_4 with lager specific surface area and more fractions of coordinated-unsaturated surface atoms and they don't have the high reflection like bulk or nanosized particles at the grain boundaries, all of which enhance the light harvesting capacity of CNNs [92]. Second, the anisotropic structure and reduced thickness of CNNs significantly shorten the perpendicular migration distance of photoinduced electron-hole pairs from the bulk to the surface, and accelerate electrons transport along the in-plane direction which promote the separation of photo-excited electrons and holes (h^+) (Fig. 2c) [93]. Third, CNNs with fewer layers provide more low-coordinated atoms due to the high ratio of surface atoms. They can induce the formation of surface defects and form active sites which facilitate not only the redox reaction on its surface but also the modification of them [94]. Finally, reducing the dimensionality of BCN to 2D CNNs makes it an effective support for guest materials to form efficient heterojunction with intimate contacts, which are generally classified as point-to-face contact, line-to-face contact and face-to-face contact between 0D, 1D, 2D materials and CNNs respectively [95]. And the efficient point-to-face contact formed between CNNs and 0D nanomaterials is just what we discuss in this review.

Therefore, in view of the excellent charge carrier separation in CNNs, it is reasonable to load 0D nanomaterials onto their surface to promote the transfer of photoinduced charge carrier and further hamper the recombination of electron-hole pairs in the bulk or on the surface of CNNs for electrostatic attraction, which decrease the photocatalytic efficiency.

3. 0D nanomaterials as enhancers of CNNs

0D nanomaterials are widely used as guest materials in the fabrication of photocatalyst to improve the performance of decorated materials. In the combination with CNNs, their smaller size can decrease the diffusion length of photoinduced electron-hole pairs, which leads to improved photocatalytic performance. On the other hand, their good dispersion on the large exposed CNNs can form abundant heterojunction interfaces without covering too many active sites, which will provide more separation channels for electrons and holes to ensure more effective separation of them [96]. So the combination of CNNs with 0D nanomaterials is an efficient strategy to further improve the photocatalytic activity of CNNs. In this section, three representative kinds of 0D nanomaterials including carbon nanodots, noble metal atoms and semiconductor nanoparticles are introduced as enhancers for the performance of CNNs and the different mechanisms are discussed in these systems.

3.1. Carbon nanodots as electrons sink

Carbon nanodots (CDots) are monodisperse graphite particles with ultrafine diameter less than 10 nm, which are typical 0D nanomaterials. They are considered as potential ingredients for the design of heterojunction photocatalysts due to their high stability, low toxicity, extraordinary up-converted photoluminescence, outstanding photo-excited electrons transfer and their important role as both excellent electron donors and acceptors contributing to efficient separation of electrons and holes [97,98]. Because their combination with CNNs showed great potential in the fabrication of environment-friendly metal-free photocatalyst and achieved considerable progress in the past years, we wrote this section for CDots specially. Synthetic methods of CDots in their combination with g-C_3N_4 were generally summarized in Table 2.

Liu et al. firstly incorporated CDots into carbon nitride to construct a highly efficient and stable photocatalyst for water splitting under the visible light in 2014 [111]. And Gao et al. theoretically studied the underlying photocatalytic mechanism of the CDots/g-C_3N_4 system [112]. They demonstrated the formation of type II van der Waals heterojunction between CDots and g-C_3N_4 that electrons transferred from CB of CNNs to CB of CDots and the role of CDots as a spectral sensitizer, which contributed to the enhanced performance of this system. Consequently, a series of studies on the combination of CDots and g-C_3N_4 were conducted for photocatalysis. Different strategies have been worked out to fabricate CDots/g-C_3N_4 system in recent years [113,114]. And transforming BCN into CNNs to combine with CDots has become an appealing method in CDots/g-C_3N_4 system fabrication for various applications. For example, a series of studies have been conducted to apply this system for H_2 evolution initially [106]. Li et al. integrated CNNs with CDots into a heterostructure via a facile solvothermal reaction, achieving the production rate of H_2 at 116.1 μmol h^{-1} under visible light [100]. Subsequently, Liu et al. coupled CDots with CNNs also by hydrothermal method for preparing the 0D/2D type photocatalyst but different synthesis ways of pristine CDots and g-C_3N_4 compared to the former study [103]. In their studies, CNNs show an enhanced photocatalytic H_2 evolution rate (28.9 μmol h^{-1}) and is 3.2 times of BCN (9.0 μmol h^{-1}) resulting from the increased specific surface area and the optimized structures. No CDots aggregation happens during the coupling of the CDots with CNNs compared to BCN and the optimized composite CNNs/CDots-0.2% achieves the H_2 production rate at 88.1 μmol h^{-1}, which is 1.91 folds of BCN/CDots-0.2% (46.3 μmol h^{-1}), indicating that the CNNs show their superiority to BCN in the interaction with CDots and contribute to the enhancement of the photocatalytic activity. Meanwhile, Jun Ong et al. successfully applied this system in CO_2 reduction. The CDots/pCN photocatalyst with 3 wt% CDots loading was found to have the highest CH_4 and CO production levels at 29.23 and 58.82 μmol h^{-1} g^{-1} after 10 h visible light irradiation, respectively [99]. The fabrication strategy was combining negatively charged CDots with positively charged protonated CNNs (pCN) through electrostatic attraction to construct 0D/2D CDots/pCN heterojunction photocatalyst, which further promoted the combination of

Table 2
Synthetic methods and physical properties of CDots in their combination with g-C_3N_4.

Precursor	Synthetic method	Diameters	Facet	Applications (Combine with g-C_3N_4)	Reference
Glucose	Ultrasonication treatment with 1.0 M NaOH solution	4.4 nm on average	(100)	CO_2 reduction	[99]
6-aminohexanoic acid and citric acid	Treat 6-aminohexanoic acid with NaOH and mix with citric acid for calcination	2–10 nm	(100)	H_2 evolution	[100]
Citric acid and ethylenediamine	Hydrothermal treatment at 180 °C for 5 h	5 nm on average	(002)	Degradation of RhB and TC-HCl	[101,102]
Rapeseed flower bee pollens	Sonication and hydrothermal treatment at 453 K for 24 h	2–5 nm	–	H_2 evolution	[103]
Graphite rods	Set two graphite rods as anode and cathode in ultrapure water and apply 30 V potential with stir for 120 h	5 nm	–	Degradation of MB	[104,105]
EDTA-2Na	Calcination in N_2	5-10 nm	–	H_2 evolution	[106]
Citric acid and branched poly (ethylenimine)	Hydrothermal treatment at 195 °C for 3 h	3.5-4.5 nm	(002)	Degradation of phenol	[107]
L-Ascorbic acid	Ultrosonication and hydrothermal treatment at 180 °C for 4 h	5 nm on average	–	H_2 evolution	[108]
Citric acid and urea	Hydrothermal treatment at 180 °C for 5 h	–	(100)	Degradation of TC	[109]
Natural graphite powder	Treat graphite with concentrated sulfuric acid, sodium nitrate and potassium permanganate, followed by 120 °C oil bath	2-7 nm	–	Oxygen reduction reaction	[110]

CDots and pCN based on the van der Waals force between them. Also, CDots/CNNs show excellent performance in the applications of contaminants degradation. For example, Hong et al. fabricated stable metal-free CDots/CNNs heterojunction and realized excellent performance in the degradation of rhodamine B (RhB) ($k = 0.01438\ min^{-1}$) and tetracycline hydrochloride (TC−HCl) ($k = 0.00642\ min^{-1}$) under visible light [102]. Zhang et al. successfully fabricated CDots/CNNs via impregnation-thermal method and 0.5 wt% CDots/CNNs composite exhibited 3.7 times faster reaction rate for phenol photodegradation than pristine CNNs [107]. All the studies above confirm that such a 0D/2D heterojunction architecture combining CDots and CNNs facilitate a lot to the improvement of photocatalytic activity under visible light.

Generally, the charge carrier transition ways can be illustrated in Fig. 3a. Excited by the visible light, photo-induced electrons transfer from the VB to CB in the CNNs and generate holes in the VB. Then the electrons can be shuttled freely to the conducting texture of CDots which efficiently retards the recombination and prolonging the lifetime of electron-hole pairs. At the same time, the π-conjugated CDots are used as a photosensitizer to sensitize CNNs and donate the electrons to the CB of CNNs, resulting in the extended visible light response region. These processes promote the photoinduced electrons and holes to separate and enrich in the CDots and VB of CNNs respectively. The electrons on the surface of CDots can realize the reduction of H^+ and CO_2 and also react with O_2 to produce $\cdot O_2^-$ which is a specie with strong oxidation. $\cdot O_2^-$ and the holes enriched in the CB of CNNs can degrade dye contaminants through oxidation reaction (Eqs. (1)–(7)).

$$CDots/CNNs \xrightarrow{hv} CDots(e^-) + CNNs\ (h^+_{VB}) \quad (1)$$

$$CNNs\ (2h^+_{VB}) + H_2O \rightarrow CNNs + 2H^+ + \frac{1}{2}O_2 \quad (2)$$

$$CDots\ (2e^-) + CO_2 + 2H^+ \rightarrow CDots + CO + H_2O \quad (3)$$

$$CDots\ (8e^-) + CO_2 + 8H^+ \rightarrow CDots + CH_4 + 2H_2O \quad (4)$$

$$CDots\ (2e^-) + 2H^+ \rightarrow CDots + H_2 \quad (5)$$

$$CDots\ (e^-) + O_2 \rightarrow CDots + \cdot O_2\text{-} \quad (6)$$

$$\bullet O_2^-/CNNs\ (h^+_{VB}) + contaminants \rightarrow oxidationproducts \quad (7)$$

In this system, the improved photocatalytic activity is attributed to the advantages of both CNNs and CDots: First, CNNs with 2D nanostructure serve as an excellent support for CDots to disperse on and efficiently suppress the aggregation of CDots on its surface. TEM of the fabricated CDots/BCN (Fig. 3b) and CDots/CNNs (Fig. 3c) demonstrate better dispersion of CDots on the surface of CNNs than BCN. Second, CDots provide efficient light harvesting and they are capable of absorbing a longer wavelength visible light and then emit the shorter wavelength light due to its up-converted photoluminescence properties, which promotes to excite CNNs to form more charge carrier [103]. Third, CDots serve as electrons sink, which prevent the recombination of photo-generated electron-hole pairs in CNNs and enhance their photocatalytic activity [99].

Therefore, when it comes to the influence factors of CDots/CNNs performance, besides the factors of CNNs discussed in section two, the characters of CDots take an important part. On the one hand, the amount of CDots deposited on the surface of CNNs influences the performance of this system to a great extent. There exists similar tendency in the above studies that the activity of CDots/CNNs gets better with the increase of CDots at the beginning but excess CDots result in the decrease in the performance of this system. Take the study by Jun Ong et al. [99] as an example, the photocurrent generate during photocatalytic process (Fig. 4a) and total CH_4 evolution in the application of CO_2 photodegradaiton (Fig. 4b) of their prepared CDots/pCN hybrids demonstrate that 3 wt% CDots/pCN exhibit the optimal performance and excess CDots on the surface of pCN decrease system activity on the contrary. This is because too much CDots would cover the active sites on the surface of CNNs and they can become recombination centers of photoinduced electron-hole pairs which are detrimental to the performance of this system [115]. Hence suitable mass ratio of CDots in CDots/CNNs should be explored to realize best performance. On the other hand, different functional groups on the surface of CDots impact on their combination with CNNs, which was discussed by Feng et al. in detail [116]. CDot with different functional groups designated as C-H-Dot, C–CHO-Dot and C–OH-Dot were combined with CNN in their study. They presented the average distance between the lowest atom and the highest atom of CNN in the normal direction of the monolayer and the average distance between CNN and CDot with different functional groups (Fig. 4c), which demonstrated the different nanostructures formed in their combination. At the same time, they calculated the binding energy (E_{bind}) of the hybrid CDot/CNN. The higher E_{bind} of C–CHO/CNN (-1.85 eV) and C–H/CNN (-1.48 eV) than double-layered CNN (-1.3 eV) proved the more stability of C-H-Dots and C-CHO-Dot on the surface of CNN. Calculation on CDot/CNN reveals that the condition whether the CDot behaved as an electron donor or acceptor can be changed by the functional groups on the CDot: As shown in Fig. 4d, the electrons are excited from CNN to CDot for C-CHO/CNN but for C-H/CNN electrons transfer from CDot to CNN. Furthermore, the CDot with -CHO and -COOH functional groups (C-CHO-Dot) is more

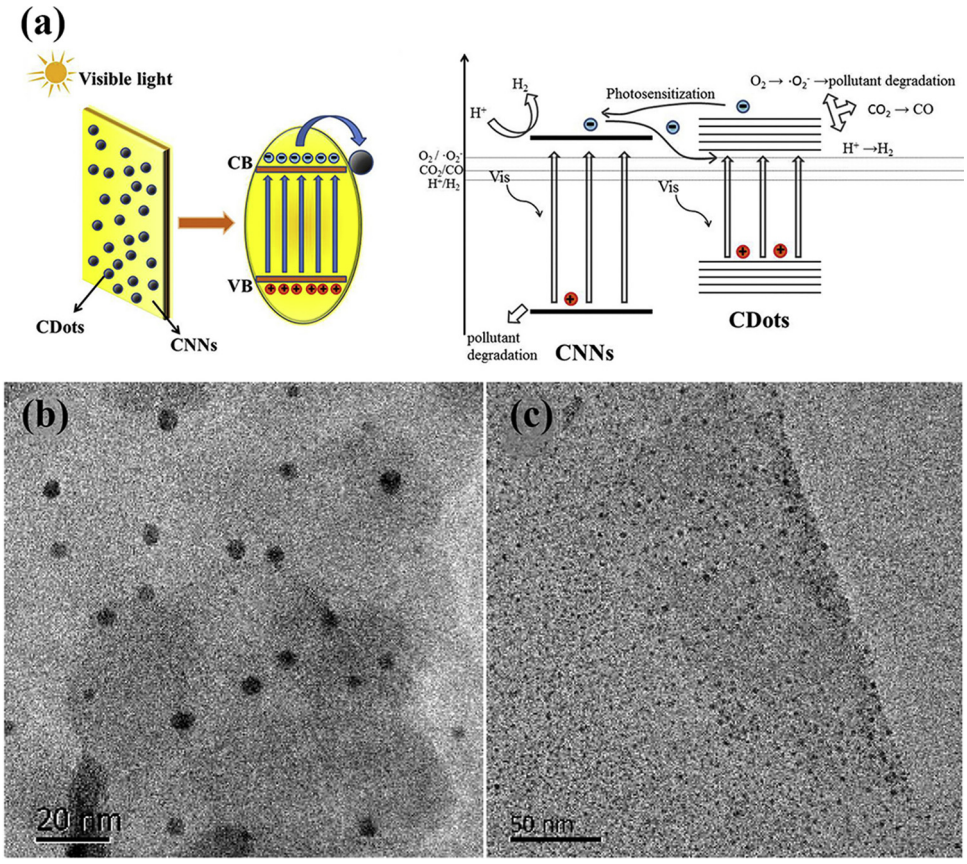

Fig. 3. (a) The charge-trasfer pathway in CDots/CNNs under visible light. TEM images of BCN/CDots-0.2% **(b)** and CNNs/CDots-0.2% **(c)** samples. Reprinted with permission from Ref. [103]. Copyright 2016 Elsevier.

suitable than that with -OH and -COOH functional groups (C-OH-Dot) to form heterojunction with g-C_3N_4, which can increase the photocatalytic efficiency through reducing the electron-hole pairs recombination rate.

3.2. Noble metal atoms with SPR effect

Noble metal atoms like silver, gold, platinum, etc. have emerged as promising materials for exploiting visible light efficiently and play as suitable co-catalyst in the fabrication of photocatalytic system for artificial photoredox reactions. The most important reason is the surface plasmon resonance (SPR) effect of noble metals, which indicates that light interacts with metal particles much smaller than the incident wavelength and leads to a plasmon that oscillates locally around the metal nanoparticles with certain frequency, contributing a lot to the significant enhancement of optical absorption in the visible light region [117,118]. This effect can induce the formation of an intensive electromagnetism, which interacts with the semiconductor and promotes the photocatalyst to form more electrons and holes. In addition, noble metals can scatter resonant photons efficiently, leading to longer optical path lengths for photons in the photocatalyst, which causes enhanced evolution rates of photoinduced charge carrier [119] and they can also act as electron sinks similar to CDots and capture photogenerated electrons to hamper the recombination of photoinduced electron and hole pairs.

Recent years it has been found that CNNs show excellent combination with noble metal atoms because the multitudinous intrinsic cavities on their surface can serve as suitable fixed points for noble atoms to form stable noble metal/g-C_3N_4 sheet (Fig. 5a). It can effectively avoid the frequent phenomenon that noble metals on the surface of low-dimensional materials move and aggregate to form clusters owing to the strong d–d interaction among them and their much weaker binding with the surface than in the bulk phase [62]. What's more, metal atoms can extend visible light absorption ability of CNNs via SPR effect to generate more photogenerated electron-hole pairs and the Schottky junction formed between them can also inhibit the recombination of photogenerated electron-hole pairs and retain the reduction ability of transferred photoinduced electrons to some extent.

Silver (Ag) atom is extremely attractive for their remarkable catalytic activity and relative cost-effectiveness [102]. So Ag/CNNs have been fabricated by different strategies for various applications. In the part of pollutants degradation, Li et al. synthesized Ag/g-C_3N_4 composite nanosheets through a simple photodeposition method for the decomposition of RhB under visible light irradiation and realized enhanced photocatalytic activity of CNNs [120]. And Jin et al. specifically compared the photocatalytic performance of Ag/CNNs with pure CNNs and Ag/BCN [121]. Ag/CNNs showed the best degradation of RhB due to the hybrid effects of Ag and CNNs that promoted the separation efficiency of photogenerated charge carrier on surface of CNNs and the localized SPR of Ag NPs. Also, a series of studies were conducted on Ag/CNNs for degradation of organic pollutants like methyl orange (MO), methylene blue (MB), neutral dark yellow GL (NDY-GL), aromatic aldehydes, etc. [122–125], in which large surface area of CNNs play crucial roles by improving the visible light absorption ability, providing abundant reactive sites and promoting photogenerated electron-hole pairs separation. The charge carrier transition ways during the degradation process can be illustrated in Fig. 5b. CNNs act as an ideal platform for Ag atoms attachment and Schottky heterojunction forms between them. Under the visible light irradiation, more electron-hole pairs are photogenerated on the surface of CNNs due to the SPR effect of Ag. Then the photoexcited electrons transfer from the CB of CNNs to Ag NPs due to the high Schottky barrier between them, which realize the

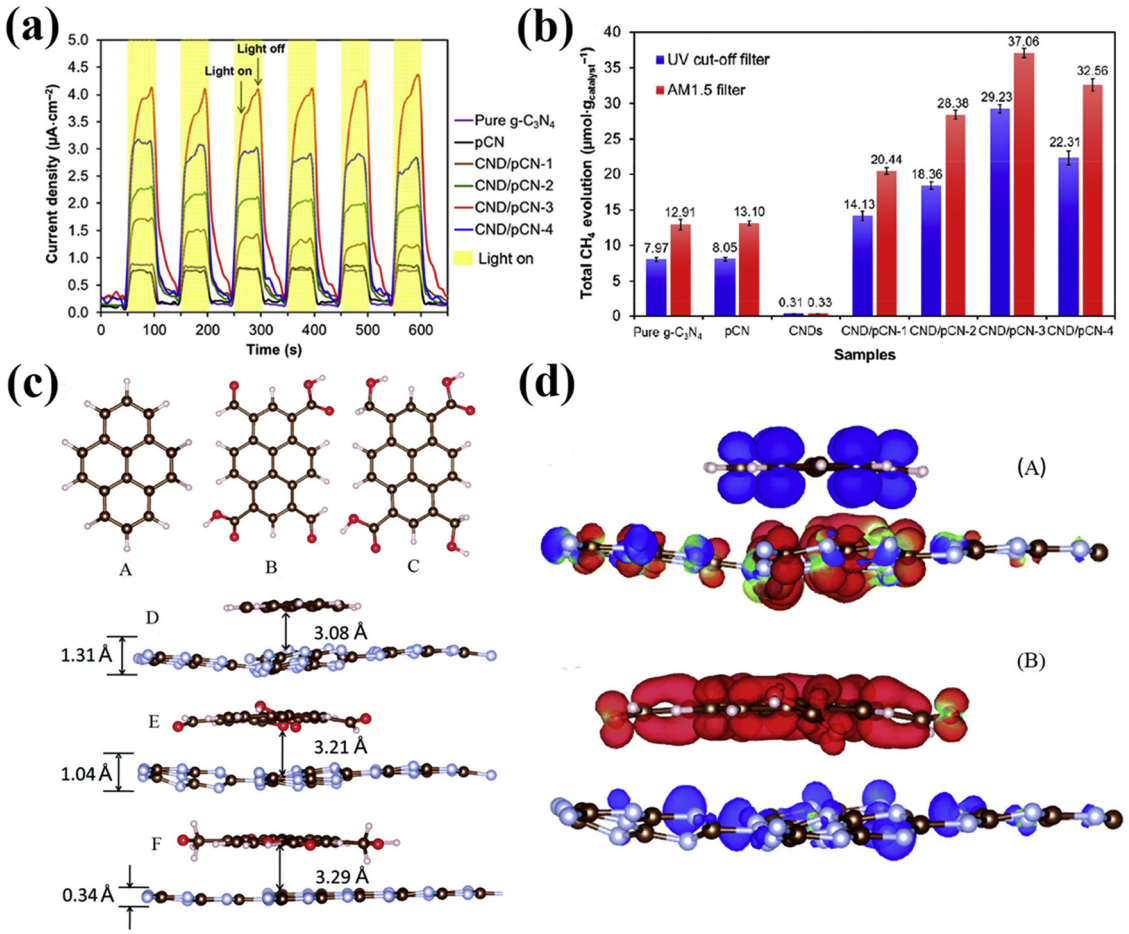

Fig. 4. (a) Transient photocurrent generation measurements of pure g-C_3N_4, pCN, and CND/pCN samples in 0.5 M Nas_2SO_4 under a bias potential of 0.5 V (vs. Ag/AgCl). **(b)** Total evolution of CH_4 with pure g-C_3N_4, pCN, CNDs, and CND/pCN samples over 10 h of reaction under visible light and simulated solar light illumination. Reprinted with permission from Ref. [99]. Copyright 2017 Springer Nature. **(c)** A–C show the structures of C–H-Dot, C–CHO-Dot, and C–OH-Dot respectively. D–F show the optimized configurations for C–H/g-C_3N_4, C–CHO/g-C_3N_4 and C–OH/g-C_3N_4. The carbon, hydrogen, nitrogen and oxygen atoms are in brown, pink, light blue and red, respectively. **(d)** Electron (red) and hole (blue) distribution of the lowest pure chargetransfer state in (A) C–H/CNN, (B) C–CHO/CNN. Reprinted with permission from Ref. [116]. Copyright 2016 Royal Society of Chemistry (For interpretation of the references to colour in this figure legend, the reader is referred to the web version of this article).

efficient charge carrier separation during the photocatalytic process. On the basis of the discussion above, the Ag NPs work as electron pools to capture the photogenerated electrons and the enriched electrons in them react with oxygen to generate $^{\cdot}O_2^-$. According to the charge carrier transition ways, Ma et al. achieved enhanced disinfection activity by combining Ag NPs and CNNs based on its production of $^{\cdot}O_2$- and $^{\cdot}OH$ (Fig. 5c) [126]. Also, Yi et al. successfully fabricated Ag/2D white-C_3N_4 (Monolayer CNN whose bang gap is larger than BCN) for H_2 evolution through reducing H^+ by the electrons with high density at the CB of 2D white-C_3N_4. The 2 wt% Ag/white g-C_3N_4 exhibited the best photocatalytic activity for H_2 evolution (17.11 μmol h^{-1}). It was demonstrated that the injection of plasmonic hot electrons from Ag improved the density of the electrons and ultrathin 2D structure led to more efficient separation of photogenerated electron and hole pairs [127].

Similarly, other noble metals were also explored to decorate CNNs. Cheng et al. firstly used CNNs prepared by ultrasonication-assisted liquid exfoliation of BCN as support to load Au NPs on them via green

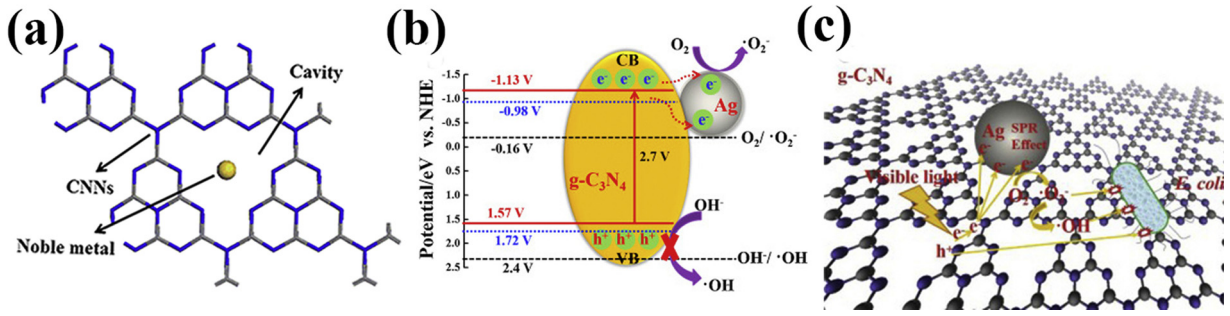

Fig. 5. (a) Cavities on the surface of CNNs for the fixsion of metal atoms. **(b)** Charge-transfer pathway of Ag/CNNs for degrading pollutants under visible light. **(c)** Charge carrier transition ways of Ag/CNNs for disinfection under visible light. Reprinted with permission from Ref. [126]. Copyright 2016 Elsevier.

photoreduction of Au (III) under visible light irradiation [128]. And Au/CNNs show superior photocatalytic activities to BCN, CNNs and Au/BCN hybrids for the decomposition of MO under visible-light irradiation. Surendar et al. fabricated Au/mp-g-C_3N_4 nanosheets through the same photoreduction strategy to efficiently degrade RhB under sunlight irradiation. Both of the enhancing photocatalytic activities resulted from the surface plasmon resonance of Au atoms and the advantages of ultrathin 2D material from g-C_3N_4 [129]. Furthermore, Nie et al. designed a new 2D material consisting of supported single-atom Au on g-C_3N_4 single layer and verified its capacity to active oxygen into super oxygen with a band gap at 1.82 eV, which demonstrated its potential as a new material in photocatalytic field [130]. Ni et al. prepared Pd NPs decorated CNNs and studied their performance in the oxidation and reduction reaction [131]. They found that Pd/CNNs displayed enhanced photocatalytic activity in oxidation removal of NO, which contributed to the electron sink Pt NPs acted as promoting the separation of photoinduced electron-hole pairs and the Schottky barrier formed between g-C_3N_4 and Pd NPs preventing the recombination of them. Conversely, the photocatalytic reduction of CO_2 by Pd/CNNs was found decreased, which resulted from the decreasing reducibility of photogenerated electrons for their transfer from the CB of CNNs to Pd NPs. This demonstrates that although the deposition of metal nanoparticles on CNNs bring increasing amount of photoinduced electrons due to the efficient separation of charge carrier, it results in weaken reducibility of the electrons and decrease the photocatalytic activity.

To further improve the photocatalytic performance of CNNs based on the noble metal decoration, bimetallic nanoparticles deposition on CNNs was explored for higher photocatalytic activity. In these bimetallic nanoparticles decorated CNNs, greatly enhanced performance was obtained through the synergistic effects between the two kinds of metal. For example, Xue et al. prepared Au/Pt/g-C_3N_4 by a facile calcination-photodeposition technique for antibiotic TC-HCl degradation [132]. In this system, Au NPs contribute to the broad absorption peak of Au/Pt/g-C_3N_4 for their SPR effect (Fig. 6a); Pt NPs serve as electron sinks and g-C_3N_4 work as an excellent mediator. As illustrated in Fig. 6b, the simultaneous electron-transfer pathway (Au→g-C_3N_4-CB→Pt) in Au/Pt/g-C_3N_4 greatly enhanced the photoinduced electron–hole pairs separation efficiency. Simultaneously, the separated electrons and holes at Pt and Au, g-C_3N_4 set off series of reactions respectively (Eqs. (8)–(12)) and realize the degradation of TC-HCl.

$$Pt\ (e^-) + O_2 \rightarrow Pt + {}^{\cdot}O_2^- \quad (8)$$

$${}^{\cdot}O_2^- + 2H^+ + e^- \rightarrow H_2O_2 \quad (9)$$

$$H_2O_2 + e^- \rightarrow {}^{\cdot}OH + OH^- \quad (10)$$

$$Au\ (h^+) + H_2O \rightarrow Au + {}^{\cdot}OH + H^+ \quad (11)$$

$$g\text{-}C_3N_4\ (h^+)/{}^{\cdot}OH + TC\text{-}HCl \rightarrow \text{degradation products} \quad (12)$$

With the synergistic effects between Au and Pt, the TC-HCl degradation rate constant of Au/Pt/g-C_3N_4 is 1.7 and 2.4 times higher than Au/g-C_3N_4 and Pt/g-C_3N_4 (Fig. 6c). Similarly, synergistic effects of Pd and Au contribute to the excellent performance of Pd/Au/CNNs for H_2 evolution and phenolic compounds degradation [133–135]. However, two factors should be noted which can influence the performance of bimetallic nanoparticles/CNNs to a great extent. The one is the deposition order of two metal nanoparticles in the fabrication process. In the preparation of Pt/Au/CNNs by Liang et al. [136], it was found that Pt species were in the form of PtO with small particle sizes when Pt was firstly loaded on the surface of CNNs (Pt@C_3N_4) while Pt species were metallic Pt NPs when they are loaded on the surface of Au/CNNs (Pt-Au@C_3N_4). By comparison, Au species were in the form of metallic Au in all Au deposited samples. So Pt-Au@C_3N_4 showed higher H_2 evolution rate than Au-Pt@C_3N_4 because PtO produced in the latter had inhibitory action on water splitting. Therefore, the surface structure of CNNs may affect the form of deposited metal nanoparticles. Importance should be attached to the metal deposition order in the fabrication of bimetallic nanoparticles decorated CNNs. The other one is the ratio of the two kinds of metal nanoparticles. For example, in photocatalyst PtCo/CNNs fabricated by Han et al. [137], the introduction of Co to form $PtCo_x$ alloys can improve their ability to capture photoinduced electrons but reduce the active sites for H_2 production because H^+ in solution is harder to be adsorbed on the surface of Co than that of Pt. So the ratio of Co to Pt should be controlled to realize more positive effects of Co than its negative effects in their combination with CNNs.

In these noble metal atoms/CNNs photocatalytic systems, CNNs behave as an excellent carrier and stabilizer promoting the photocatalytic performance to some extent due to its large surface area and special p-bonded planar structure, which emphasize the potential of CNNs as support of noble metal nanoparticles for enhanced photocatalytic activity. Also, the deposited noble metal atoms serve as a suitable enhancer for their optical properties and their loading amount presents the similar tendency to carbon nanodots because excess noble metal atoms will cover the active sites on the surface of CNNs too much and even become the center for photocatalytic electron-hole pairs recombination.

3.3. Semiconductor nanoparticles by forming heterojunction with CNNs

Semiconductor nanoparticles we discuss here indicate the semiconductive nanomaterials with particle sizes smaller than 100 nm (0D) [138]. They have received extended applications in photocatalyst fabrication field due to their high specific surface areas, high conductivity and easy dispersion, which benefit their combination with CNNs. Three aspects including mechanisms, fabrication and typical examples of semiconductor nanoparticles/CNNs are discussed specifically.

3.3.1. Photocatalytic mechanisms of semiconductor nanoparticles/CNNs

As guest materials in the photocatalyst system based on CNNs, semiconductor nanoparticles play their role in improving the photocatalytic activity through forming heterojunction with CNNs and promoting the photoinduced electron-hole pairs separation primarily. It can be seen from recent researches that the main types of the heterojunction are type II heterojunction and Z-scheme heterojunction.

For example, typical type II heterojunction is formed in Ag_2CO_3 NPs/CNNs fabricated by Tonda et al. [139]. The charge-transfer pathways are depicted in Fig. 7a. Under visible light, both CNNs and Ag_2CO_3 NPs absorb photons with higher energy than their band gap energy, which excite the electrons in the VB to the CB and leave holes in the VB. The excited electrons in the CB of the CNNs can be easily transferred to the CB of the Ag_2CO_3 NPs due to their more negative potential (-1.3 eV vs. NHE) than Ag_2CO_3 NPs (+ 0.36 eV vs. NHE). At the same time, the holes generated in the VB of Ag_2CO_3 NPs would transfer to the VB of CNNs because its potential (+ 2.68 eV vs. NHE) is more positive than CNNs (+ 1.4 eV vs. NHE). The transition of photoinduced charge carrier can be promoted by the inner electric field established at the heterojunction interfaces and the photogenerated electron-hole pairs are efficiently separated. Finally, the enriched electrons in the CB of Ag_2CO_3 can react with dissolved oxygen to form ${}^{\cdot}O_2^-$ and the enriched holes in the VB of CNNs react with H_2O to generate ${}^{\cdot}OH$, which contribute to the oxidation of pollutants [140]. Different from Ag_2CO_3 NPs/CNNs, Z-scheme heterojunction is formed in the TiO_2 NPs/g-C_3N_4 fabricated by Jo et al. [141]. The charge-transfer pathways are illustrated in Fig. 7**b**. First, both TiO_2 and CNNs produce photogenerated electro-hole pairs under visible light. Second, photogenerated electrons in the CB of TiO_2 transfer to the VB of CNNs and recombine with the photogenerated holes, which realize the accumulation of electrons in the CB of g-C_3N_4 and holes in VB of TiO_2.

Therefore, these two types of heterojunction both realize to promote the separation efficiencies of photoinduced electron-hole pairs. But compared to type II heterojunction, Z-scheme heterojunction can avoid the decrease in the redox ability of photoinduced electrons and holes

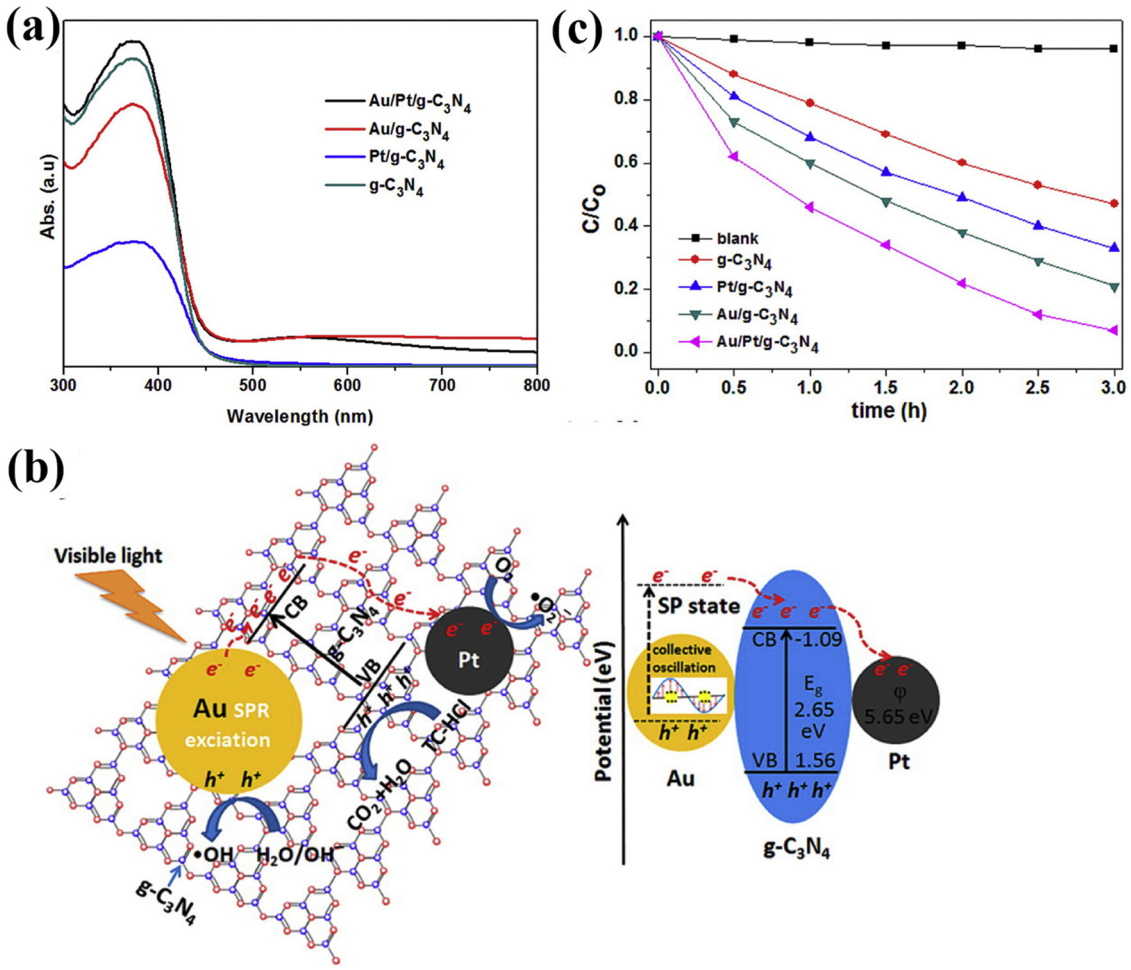

Fig. 6. (a) UV–vis diffuse reflectance spectra of g-C_3N_4, Pt/g-C_3N_4, Au/g-C_3N_4, and Au/Pt/g-C_3N_4 nanocomposites. **(b)** The photocatalytic activities towards TC-HCl degradation with g-C_3N_4, Pt/g-C_3N_4, Au/g-C_3N_4, and Au/Pt/g-C_3N_4 nanocomposites. **(c)** Proposed photocatalytic mechanism for degradation of TC-HCl by Au/Pt/g-C_3N_4 nanocomposites under visible light irradiation. Reprinted with permission from Ref. [132]. Copyright 2015 American Chemical Society.

resulting from the charge carrier transition in type II heterojunction, which contribute to higher photocatalytic activity relatively.

3.3.2. *Nanostructure fabrication of semiconductor nanoparticles/CNNs*

The fabrication of semiconductor nanoparticles/CNNs has been developed in recent years. Compared to conventional phtocatalyst synthesis, the control on the microstructure of loaded semiconductor nanoparticles is crucial to photocatalyst performance in the preparation progress. Therefore many fabrication methods have been explored to realize smaller size and better distribution of semiconductor nanoparticles on CNNs.

In-situ growth method is widely used in preparation of semiconductor nanoparticles/CNNs, especially for the combination of metal salt with CNNs. The precursor of metal salt can easily deposit on the surface of CNNs and then be transformed to metal salt nanoparticles after further treatment. For example, Ye et al. successfully fabricated vanadate QDs/CNNs through in situ method [142]. Take $AgVO_3$ for example, the process can be illustrated in Fig. 8a. The surface of CNNs

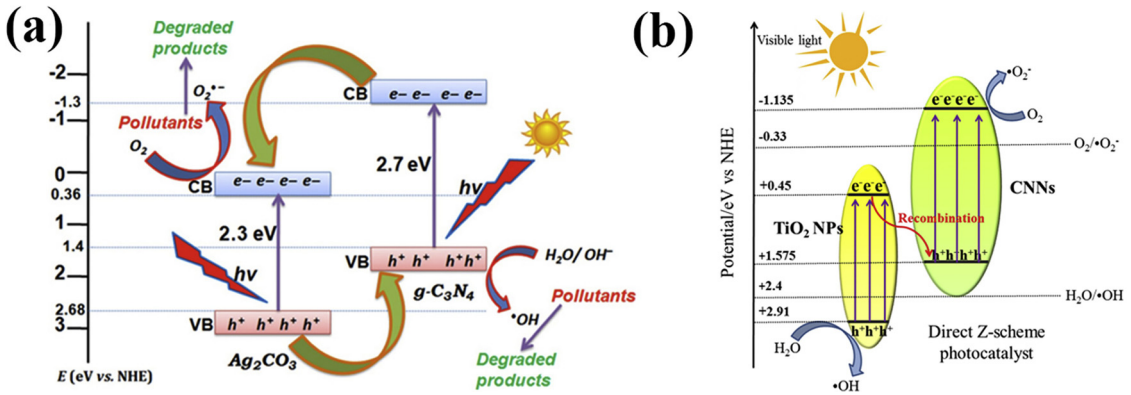

Fig. 7. (a) Schematic photocatalytic reaction process and charge transfer of the Ag_2CO_3/g-C_3N_4 with typr II heterojunctions under visible light irradiation. Reprinted with permission from Ref. [139]. Copyright 2015 Elsevier. **(b)** The schematic diagram of the Z-scheme heterojunction in TiO_2/g-C_3N_4 composite photocatalysts.

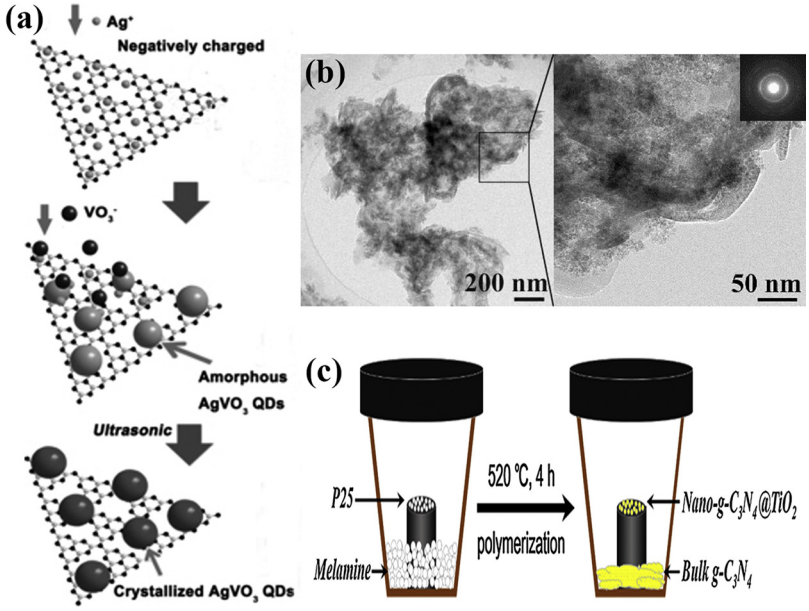

Fig. 8. (a) Formation mechanism of the $AgVO_3$ QDs/CNNs heterojunction. Reprinted with permission from Ref. [142]. Copyright 2017 John Wiley & Sons, Inc. **(b)** TEM images of TiO_2 NPs/CNNs composite fabricated after seeding with 1 mM $TiCl_4$ dilute aqueous solution. Reprinted with permission from Ref. [151].Copyright 2015 Elsevier. **(c)** Innovative fabrication of nanostructured g-C_3N_4/TiO_2 through vapor deposition of g-C_3N_4 onto TiO_2 NPs. Reprinted with permission from Ref. [152].Copyright 2018 Elsevier.

can easily absorb Ag^+ due to its negative charge with an average zeta potential of about -17.0 mV and the nitrogen-coordinating sites in their tri-s-triazine units can also capture metal, both of which lead to robust fixation and high dispersion of Ag^+. Then in situ $AgVO_3$ QDs formed after the introduction of VO_3^- and they present amorphous for their distinct crystalline structures and the growth was confined by the N-binding effect of CNNs. Lastly the amorphous $AgVO_3$ transformed to crystalline QDs (3–5 nm) with the treatment of ultrasonication. Also, Zhang et al. constructed a-AgSiO/CNNs through in situ precipitation [143]. In the process, CNNs was dispersed in $AgNO_3$ solution and sonicated to realize the better deposition of Ag^+ on the surface of CNNs. Then $Na_2SiO_3{\cdot}9H_2O$ was added for reaction to produce a-AgSiO. In the obtained samples, ultrafine a-AgSiO (~5.2 nm) uniformly dispersed on the entire surface of hierarchical ultrathin CNNs. In-situ growth method was used in the fabrication of β-Ag_2MO_4/g-C_3N_4 [144], g-C_3N_4/Bi_2WO_6 [145] and AgCl@g-C_3N_4 [146].

Hydrothermal/solvothermal method is a suitable way to combine metal sulfide or metal oxide with CNNs, such as MoS_2/g-C_3N_4 [147], ZnS/CNNs [148], NiS/CNNs [149] and SSOP/PCNNS [150]. For example, ZnS/CNNs was prepared through a one-pot hydrothermal method by heating the mixture of $Zn(Ac)_2{\cdot}2H_2O$, $Na_2S{\cdot}9H_2O$ and g-C_3N_4 [148]. In the obtained sample, g-C_3N_4 showed lamellar stacking structure and ZnS was a spherical-like nanoparticle with size around 30.65 nm. Further, this method was improved by Li et al to construct TiO_2/g-C_3N_4 hybrid nano-architectures [151]. In the study, Seed-induced growth approach was used to realize readily controlling on the microstructure and morphology of TiO_2 NPs. They firstly immersed CNNs into $TiCl_4$ dilute aqueous solution to realize the deposition of TiO_2 nuclei on the surface of CNNs, which was called seeding process, before dispersing them in a solvent containing Ti precursor for hydrothermal treatment. Results indicated that "seeding" endowed CNNs with anchoring sites toward the heterogeneous nucleation growth of TiO_2, and the distribution of loaded TiO_2 on its surface could be controlled by tuning the amount of nucleation in the dispersion. Fig. 8b shows the TiO_2 NPs/CNNs composite fabricated after seeding with 1 mM $TiCl_4$ dilute aqueous solution. Through this method they realized to maintain regular shapes, narrow size distributions and control the structures of TiO_2 NPs on the surface of CNNs to design a more suitable structure for harvesting visible light, shorting the charge transport distance and providing a large contact area for fast interfacial charge separation and photocatalytic reactions.

Calcination method is another method in which semiconductor nanoparticles are mixed with g-C_3N_4 or the precursor of g-C_3N_4 for thermal treatment. Some of its applications in combining CNNs with metal oxide are innovative. For example, Tan et al. fabricated nanostructured g-C_3N_4/TiO_2 through vapor deposition of g-C_3N_4 onto TiO_2 NPs [152]. The specific process is shown in Fig. 8c. Melamine and TiO_2 were put separately in a covered crucible for calcination. And CNNs successfully deposit on TiO_2 NPs during the sublimation and polymerization reaction of melamine. The obtained samples showed that TiO_2 NPs were 10 ~ 20 nm in diameter and CNNs were 20 nm in thickness. In the fabrication of Co_3O_4 QDs/g-C_3N_4 by Zhang et al. [153], g-C_3N_4 and Co_3O_4 QDs were mixed in absolute ethanol and the solution was evaporated under constant stirring. After that, the dried mixture was collected and annealed under air, which realized homogeneous deposition of Co_3O_4 QDs on the surface of CNNs. Also, calcination method was used in the fabricated of ZnS@g-C_3N_4 [154], Fe-doped C_3N_4/WO_3 [155] and QDs@ Flake g-C_3N_4 [156].

Otherwise, ultrasonication treatment has ingenious applications in semiconductor nanoparticles/CNNs photocatalyst fabrication. Wang et al. combined $BiFeO_3$ NPs and g-C_3N_4 by facilely treating them with ultrasonication and stir [157]. The formation process of g-C_3N_4/$BiFeO_3$ nanocomposites was discussed concretely: First, g-C_3N_4 and $BiFeO_3$ powder dispersed in methanol with ultrasonication to form CNNs and broken $BiFeO_3$ NPs. Second, small $BiFeO_3$ NPs attached to the surface of CNNs by the effects of the surface charge and $BiFeO_3$ NPs tended to aggregate along a certain direction in order to minimize the overall energy of the reaction system, which could be explained by the "oriented attachment" mechanism [158]. Third, the primary self-aggregate $BiFeO_3$ NPs recrystallized according to the Gibbs-Thomson law and the surface energy was further decreased to make the as-prepared spindle-like $BiFeO_3$ NPs much more stable [159]. Similarly, Zeng et al. incorporated Ni_2P NPs onto CNNs by mixing two immiscible solutions (Ni_2P dispersed in hexane and g-C_3N_4 dispersed in *N,N*-Dimethylformamide) under constant sonication and stir, which maintained the desired size and morphology of Ni_2P NPs (10.3 nm in size) [160]. Through this method, tight heterojunction interfaces were constructed between 0D Ni_2P NPs and CNNs. These methods demonstrate the effectiveness of sonication in the combination of 0D nanoparticles and CNNs.

3.3.3. Typical semiconductor nanoparticles/CNNs

Silver containing compounds show high utilization of visible light and semiconductor-like feature, which expand their applications in

Table 3
A summary of recently reported Ag containing compounds/CNNs photocatalysts including their fabrication strategies, applications and charge-transfer mechanism.

Photocatalytic system	Fabrication strategy	Preparation of CNNs (Precursor/Exfoliating method)	Applications	Optimum component/ Performance	Charge-transfer mechanism	Reference
Ag_2CO_3/g-C_3N_4	In situ precipitation	Melamine/Liquid exfoliation	Degradation of RhB and 4-CP	10 wt% Ag_2CO_3/ ~ 99% degradation in 30 min for RhB	Type II heterojunction	[139]
Ag_2O/ g-C_3N_4 NSs	Chemical precipitation	Urea/ Ultrasonication	Degradation of MO	71.4 wt% Ag_2O/ 95% degradation in 120 min	P-N heterojunctions under UV, electrons transfer to Ag^0 under NIR	[161]
Ag_2WO_4/ g-C_3N_4 NS	Deposition-precipitation	Melamine/Thermal oxidation etching	Degradation of RhB and MO	20 wt% Ag_2WO_4/ ~ 100% degradation in 20 min for RhB, 85% degradation in 50 min for MO	Electrons transfer from CB of CNNs to CB of Ag_2WO_4	[70]
AgCl@g-C_3N_4	Deposition-precipitation	Melamine/ Ultrasonication	CO_2 reduction	1 wt% AgCl/Production rate of methane is about 25.67 μmol/g	Z-scheme heterojunction	[146]
Ag_3PO_4/CNNs	Deposition-precipitation	Melamine/ Ultrasonication	Degradation of MO	50 wt% Ag_3PO_4/ 85% degradation in 12 min	Type II heterojunction	[162]
Ag_3PO_4/H-C_3N_4	Electro-statically driven assembly	Cyanuric acid and melamine/–	Water oxidation	–/19 μmol/L of O_2 production in 14 min	Z-scheme heterojunction	[163]
a-AgSiO/ CNNS	In situ precipitation	Urea/ Thermal oxidation etching	Degradation of RhB and TC	CNNS-500 mg/100% degradation in 15 and 140 min under UV and VL for RhB, ~ 97.5%and ~ 90.5% degradation in 40 and 140 min under UV and VL for TC	Type II heterojunction	[143]
β-Ag_2MO_4/ g-C_3N_4	Deposition-precipitation	Melamine/ Ultrasonication	Degradation of RhB, MB and MO	37.5 wt% β-Ag_2MoO_4/ 99.4% degradation in 60 min for RhB, 84.4% degradation in 60 min for MO, 100% degradation in 60 min for MB	Type II heterojunction	[144]
Ag_2NCN NPs/ g-C_3N_4	Thermal annealing and in situ precipitation	Urea/Calcination	Degradation of MO and MB	10 wt% Ag_2NCN/92% degradation in 12 minutes for MO and 97.4% in 6 minutes for MB	Type II heterojunction	[164]
$AgVO_3$ QDs/ g-C_3N_4	Ultrasonic reaction route	Urea/Ultrasonication	Disinfection of Salmonella	–/96.4% bactericidal efficiency	Type II heterojunction	[165]
Vanadate quantum dots ($AgVO_3$)/ g-C_3N_4 NSs	In situ growth	Dicyandiamide/ Oxidation etching	Degradation of MO	30 wt% $AgVO_3$/ 54% degradation in 60 min	Type II heterojunction	[142]

photocatalytic field. So the combination of silver containing compounds nanoparticles with CNNs achieved great progress in recent years. Herein, we summarize some Ag containing compounds/CNNs photocatalysts. Their fabrication strategies and different charge carrier transition mechanisms are listed in Table 3. For example, in the study of Yang et al. combining Ag_3PO_4 with g-C_3N_4, it was found that Ag_3PO_4 NPs were smaller and more uniform on the surface of H-C_3N_4 (nanosheets structure) than M-C_3N_4 (bulk-like morphology) and meso-C_3N_4 (mesoporous structure), which contributed to the best performance of Ag_3PO_4/H-C_3N_4 for water oxidation [163]. This indicates the confinement of CNNs on the growth of Ag_3PO_4 NPs. Similarly, in Ag_2O/CNNs fabricated by Li et al., CNNs could not only perform as the support to form heterostructure with Ag_2O but also be employed as dispersants to confine their aggregation, leading to uniform deposition of ultrafine Ag_2O NPs on the surface of CNNs [161]. Li et al. fabricated Ag_2WO_4/CNNs heterostructured photocatalyst and the optimum photocatalytic activity achieved at 26.5 times higher than Ag_2WO_4/BCN, which was attributed to the fast interfacial charge transfer and increased lifetime of photoinduced charge carrier brought by the combination of CNNs with Ag_2WO_4 NPs and demonstrated the crucial role CNNs played in the system for the improved photocatalytic activity [70]. a-AgSiO/CNNs-500 composite prepared by Zhang et al. showed about 36 and 13 times higher photocatalytic activity than that of CNNs toward the degradation of RhB and tetracycline (TC) due to the fully exposed reactive sites, well-defined nanostructures of CNNs, synergistic interactions of heterojunction with strong interfacial coupling effect and abundant heterojunction interfaces provided by the intimate and maximum coupling interfaces between ultrasmall a-AgSiO NPs and CNNs [143]. The series of studies above proved the systems that CNNs act as an advantageous support and the guest materials Ag based compounds nanoparticles serve as enhancers show great potential in photocatalytic applications.

Metal sulfide has been explored to combine with g-C_3N_4 recent years [166–168]. Especially, metal sulfide nanoparticles can receive benefit from its combination with CNNs in the photocatalyst fabrication. For example, CdS is an ideal semiconductor photocatalyst with good response to the visible light due to its narrow band gap (2.14 eV), but its applications are greatly limited for the oxidation of S^{2-} by photogenerated holes during the photocatalytic process, which is also a limit to most sulphide in the photocatalytic applications [169]. In this respect, Xu et al. took strategies to load CdS NPs on the CNNs and realized to improve the photocatalytic activity in the degradation of MO [170]. The photocorrosion degree of CdS in this system was evaluated. 73.7 wt% CdS/CNNs was found to maintain high reactive activity with the MO degradation efficiency of 93.8% even after 5 cycles (Fig. 9a), which demonstrated the high stability of CdS NPs/CNNs. And they detected the Cd^{2+} concentration dissolved in the supernatant after photocatalytic reaction by atomic absorption spectroscopy and determined as 22.89, 19.75 and 12.88 mg/L for pure CdS, 73.7 wt% CdS/CNNs and 30.3 wt% CdS/CNNs, respectively. So the photocorrosion of CdS could be suppressed via the combination with CNNs to some extent. In ZnS@g-C_3N_4 composite photocatalyst fabricated by Xue et al., it was found that the crushed and exfoliated CNNs could provide more active sites to adsorb RhB molecules and greatly facilitated its photocatalytic degradation [154]. Furtherly, according to the study that ZnS can improve the photocatalytic activity of CdS by forming various composites like $Zn_{1-x}Cd_xS$ with CdS [171], nano-heterostructures of $Zn_{1-x}Cd_xS$ ($0 < x < 1$) NPs with small CNNs ($Zn_{0.8}Cd_{0.2}S$/CN) were prepared and exhibited even much better performance (~ 99% degradation within 15 min) than ZnS@g-C_3N_4 (95.3% degradation within 80 min) in the degradation of RhB [172]. Just as important, thereinto $Zn_{0.8}Cd_{0.2}S$/CN interacts with CNNs to promote the charge carrier transfer between them and surmount the corrosion-prone shortcoming of it. Lu et al. successfully deposited NiS on exfoliated C_3N_4 nanosheets

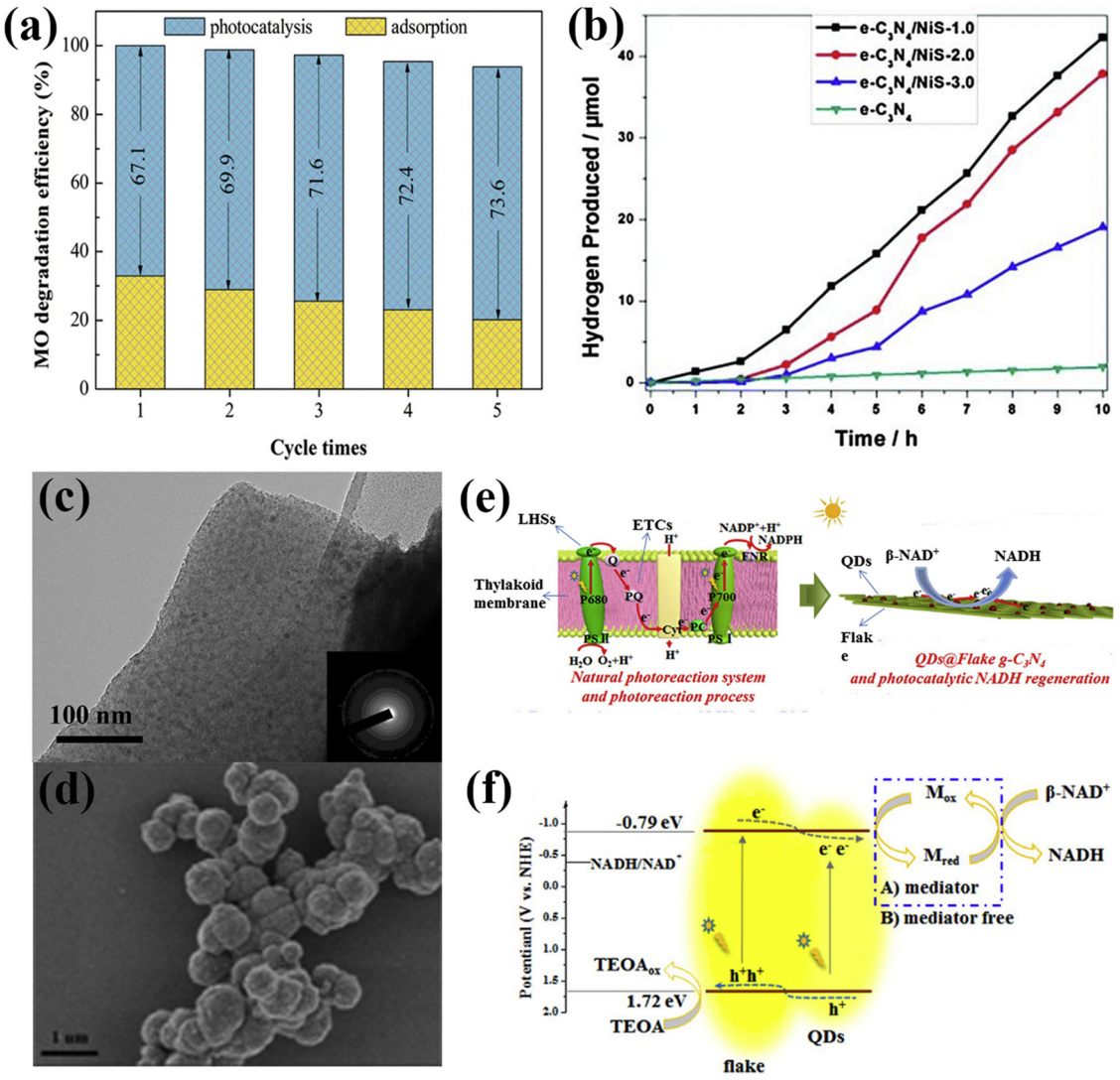

Fig. 9. (a) Cycling tests on MO degradation using CSCN 733 as photocatalyst, Reprinted with permission from Ref. [170]. Copyright 2017 Elsevier. **(b)** Influence of the NiS content on the photocatalytic activity of e-C3N4 and e-C3N4/NiS. Reprinted with permission from Ref. [149]. Copyright 2017 Royal Society of Chemistry. **(c)** The TEM images of 32 wt% $Cd_{0.5}Zn_{0.5}S@C_3N_4$. **(d)** The SEM image of pure $Cd_{0.5}Zn_{0.5}S$. Reprinted with permission from Ref. [189]. Copyright 2016 Royal Society of Chemistry. **(e)** Evolution from natural photoreaction system to QDs@Flake g-C_3N_4 for photocatalytic regeneration of NADH in the absence and presence of a mediator. **(f)** Charge-transfer pathway in QDs@Flake g-C_3N_4. Reprinted with permission from Ref. [156]. Copyright 2017 American Chemical Society.

(e-C_3N_4, with thickness of about 3 nm) for H_2 evolution and achieved at H_2 production of 4.2 μmol h^{-1} compared to no H_2 production by NiS NPs [149]. The performance of e-C_3N_4 and NiS/e-C_3N_4 can be seen from Fig. 9b. The outstanding photocatalytic performance of NiS/e-C_3N_4 results from the large surface area and improved electron transportability. On the other hand, the condition that higher loading of NiS NPs decreases the photocatalytic activity of the composite may be for that excess covered NiS NPs leads to a decrease in the surface active sites of e-C_3N_4 nanosheets and shield the incident light which prevents the generation of electron-hole pairs. Also, MoS_2 NPs, $Cu_{1.96}S$ NPs and In_2S_3 NPs were evenly dispersed on the surface of CNNs and presented higher performance in the degradation of dye contaminants and ciprofloxacin than their component materials [147,173,174]. CNNs inhibited the aggregation of these nanoparticles on the surface and endowed the systems with high stability during photocatalytic process.

Metal oxide nanoparticles are also suitable guest materials to combine with CNNs. For example, TiO_2 NPs/CNNs fabricated by Yan et al. realized H_2 evolution rate at 154 μmol h^{-1} [175]. In this photocatalyst, CNNs serve as template and guidance for the heterogeneous nucleation of anatase TiO_2. Fe_2O_3/g-C_3N_4 synthesized by Lin et al. achieved to degrade 90% 4-nitrophenol within 40 min visible light irradiation [69]. It was demonstrated that CNNs with a layered structure could provide numerous nucleation sites for the growth of Fe_2O_3, leading to the homogeneous dispersion of Fe_2O_3 NPs on their surface. Anandan et al. successfully loaded p-type Cu_2O NPs onto n-type CNNs through reduction of $CuSO_4$ by $NaBH_4$ [176]. Results demonstrated that the sheet or platelet-like morphology of polymeric g-C_3N_4 changed to crumpled surfaces upon Cu_2O anchoring and the Cu_2O-CNNs showed the high liberation of hydrogen, viz. 842 μmol h^{-1} g^{-1} after 48 h illumination. Also, WO_3/CNNs photo-Fenton system [155,177,178], SnO_2 NPs/CNNs [150] exhibited excellent performance in p-nitrophenol degradation, CO_2 reduction and gaseous iso-isopropanol oxidation.

Moreover, many other semiconductor nanoparticles have been combined with CNNs and achieved enhanced photocatalytic activity, such as bismuth containing compounds, Ni_2P, novel metal organic framework et al. Here we summarized them in Table 4.

Most noteworthy, as smaller structure of nanoparticles, 0D semiconductor quantum dots have caught increasing attention in their combination with CNNs recently [185]. They possess stronger redox ability, higher specific surface areas, shorter charger-transfer length

Table 4
Summarization of different kinds of semiconductor nanoparticles combining with CNNs.

Photocatalytic system	Fabrication strategy	Preparation of CNNs (Precursor/Exfoliating method)	Applications	Optimum component/ Performance	Charge-transfer mechanism	Reference
Bi_2MoO_6/C_3N_4	Solvothermal reaction	Melamine/ Ultrasonication	Degradation of RhB	70 wt% Bi_2MoO_6/ 84.98 % degradation in 120 min	Type II heterojunction	[179]
g-C_3N_4/ Bi_2WO_6	In situ growth	Urea/ Sonication	Degradation of RhB	70 wt% Bi_2WO_6/0.054 min^{-1}	Type II heterojunction	[145]
$BiFeO_3$/ g-C_3N_4	Deposition-precipitation	Melamine/ Ultrasonication	Degradation of MO	50 wt% $BiFeO_3$/ Better than pure g-C_3N_4 or $BiFeO_3$	Type II heterojunction	[157]
Ni_2P/g-C_3N_4 nanosheets	Solution-phase self-assembly	Urea/Ultrasonication	H_2 evolution	3.5 wt% Ni_2P/474.7 μmol g^{-1} h^{-1}	Electrons transfer from the CB of g-C_3N_4 to Ni_2P	[160]
Ni_2P/g-C_3N_4	hydrothermal method	Melamine/Thermal oxidation etching	H_2 evolution and bacterial inactivation	1wt% and 10 wt% Ni_2P/ 22 and 10 times higher than pure g-C_3N_4 respectively	Z-scheme heterojunction	[180]
$Ni_{12}P_5$ NPs/ CNNs	Solution-phase approach	Urea/Sonication	H_2 evolution	5 wt% $Ni_{12}P_5$/535.7 μmol g^{-1} h^{-1}	Electrons transfer from the CB of g-C_3N_4 to $Ni_{12}P_5$	[181]
g-C_3N_4/N doped-$LaTiO_3$	Sol-gel polymerized Complex method	Urea/Calcination	Degradation of RhB and 2,4-DCP	60 wt% N-$LaTiO_3$/90% degradation in 40 min for RhB, 84% degradation in 50 min for 2,4-DCP	Type II heterojunction	[182]
CFB/ NH_2-MIL-125 (Ti)	Solvothermal method	Thiourea/Thermal strip oxidation	H_2 evolution	10 wt% CFB/1.123 mmol h^{-1} g^{-1}	Z-scheme heterojunction	[183]
ZIF-8/g-C_3N_4	Ultrasonic in-situ synthesis	Melamine/ Ultrasonication	Degradation of TC, RhB and MO	3.0 wt% ZIF-8/1.69, 3.96 and 4.10 times higher than g-C_3N_4 respectively	Electrons transfer from the CB of g-C_3N_4 to methylimidazole ring of ZIF-8	[184]

and quantum confinement compared to larger particles, which greatly facilitate their photocatalytic applications [186,187]. But they are limited by their easy photocorrosion, self-aggregation and high photoluminescence [188]. Therefore, combining semiconductor quantum dots with CNNs can perfectly make up for their defects and show a broader trend in photocatalyst fabrication.

Many fabrication strategies of semiconductor nanoparticles/CNNs photocatalysts attempt to decrease the size of semiconductor nanoparticles to realize higher photocatalytic efficiency. For example, in $AgVO_3$ QDs/CNNs photocatalyst, $AgVO_3$ realize better dispersity and smaller sizes on the surface of CNNs and intimate type II heterojunction is formed between them, which contribute to their excellent performance in MO degradation [142] and *Salmonella* disinfection [165] under visible light. Co_3O_4 QDs/CNNs fabricated by Zhang et al. realized efficient water oxidation [153]. It showed 4 times higher than pristine g-C_3N_4 in produced O_2 amount, which contributed to the higher specific surface areas of Co_3O_4 QDs and CNNs, shorter charger transport paths between them and the low charge carrier recombination rates. Yao et al. located $Cd_{0.5}Zn_{0.5}S$ QDs on 2D g-C_3N_4 ultrathin microribbons to construct 0D/2D structure realizing efficient H_2 generation [189]. Results showed that the nano-sized $Cd_{0.5}Zn_{0.5}S$ QDs with the size around 5 nm presented a sufficient and well-distributed contact with g-C_3N_4, which led to efficient electronic mobile channel and short charge transition path, thus resulting in increased reactive sites. The image of $Cd_{0.5}Zn_{0.5}S@C_3N_4$ (Fig. 9c) and pristine $Cd_{0.5}Zn_{0.5}S$ sample prepared under the same hydrothermal condition without g-C_3N_4 (Fig. 9d) demonstrated the latter existed significant aggregation but combining with CNNs could effectively inhibit it. Moreover, $Cd_{0.5}Zn_{0.5}S@C_3N_4$ exhibited much higher performance in H_2 photogeneration than $Cd_{0.5}Zn_{0.5}S$@bulk C_3N_4 samples. These results proved that the 2D sheet-like g-C_3N_4 microribbons could serve as an effective host support and interact with $Cd_{0.5}Zn_{0.5}S$ QDs to give rise to a higher photocatalytic activity. Yang et al. explored a 2D isotype heterojunction photocatalyst, termed as quantum dots@flake graphitic carbon nitride (QDs@Flake g-C_3N_4), for NADH regeneration like the process on thylakoid membrane, by one-step calcination using cyanamide-treated cyanuric acid-melamine (CM) complex as starting material (Fig. 9e) [156]. They innovatively replicate both the functional and structural properties of the natural photoreaction system through this 0D/2D system, the two types of g-C_3N_4 (i.e., QDs and flake), heterojunction interfaces between them and 2D flake structure mimic the functional components of light harvesting systems (LHSs, i.e., photosystem I and photosystem II), electron transport chains (ETCs) and thylakoid membrane, respectively. And there formed type II heterojunction between the QDs moiety and flake moiety, which promote the separation of photoinduced charge carrier and the accumulation of electrons in the CB of QDs moiety and holes in the VB of flake moiety (Fig. 9f). The 2D topological structure of QDs@Flake g-C_3N_4 also contribute to the accumulation of electrons in the CB of QDs moiety because 2D direction transfer of photogenerated electrons in the flake moiety benefit their rapid migration to QDs moiety. So QDs@Flake g-C_3N_4 shows remarkably improved performance in visible light harvesting and charge separation, and achieves photocatalytic NADH regeneration at a regeneration yield of up to 40%.

Therefore, in the combination of 0D semiconductor nanoparticles and CNNs, the typical nanostructure of CNNs provides a suitable scaffold for contacting with other semiconductor nanoparticles and is propitious to form promising interfaces with them to improve the rate of charge transfer. At the same time, they are employed as suitable dispersants to confine the aggregation of semiconductor nanoparticles, leading to ultrafine nanoparticles uniformly packed throughout their surface. At the same time, the introduction of semiconductor nanoparticles realizes more heterojunction interfaces by minimum amount of guest materials to realize a giant leap in the performance of the photocatalytic system.

4. Multicomponent complex systems based on 0D nanomaterials/ CNNs

Recently, increasing efforts have been made to design multicomponent complexed photocatalytic systems with more efficient performance based on the 0D nanomaterials/CNNs structure presented above. The strategies in the design of more complex systems mainly include three aspects: enlarge the specific surface area to provide more active centers, enhance the visible light absorption and further promote the charge carrier separation through the interaction of several components. Herein we introduce three kinds of ternary systems with characteristic nanostructures.

The first kind of system is dual nanoparticle co-loaded CNNs. These

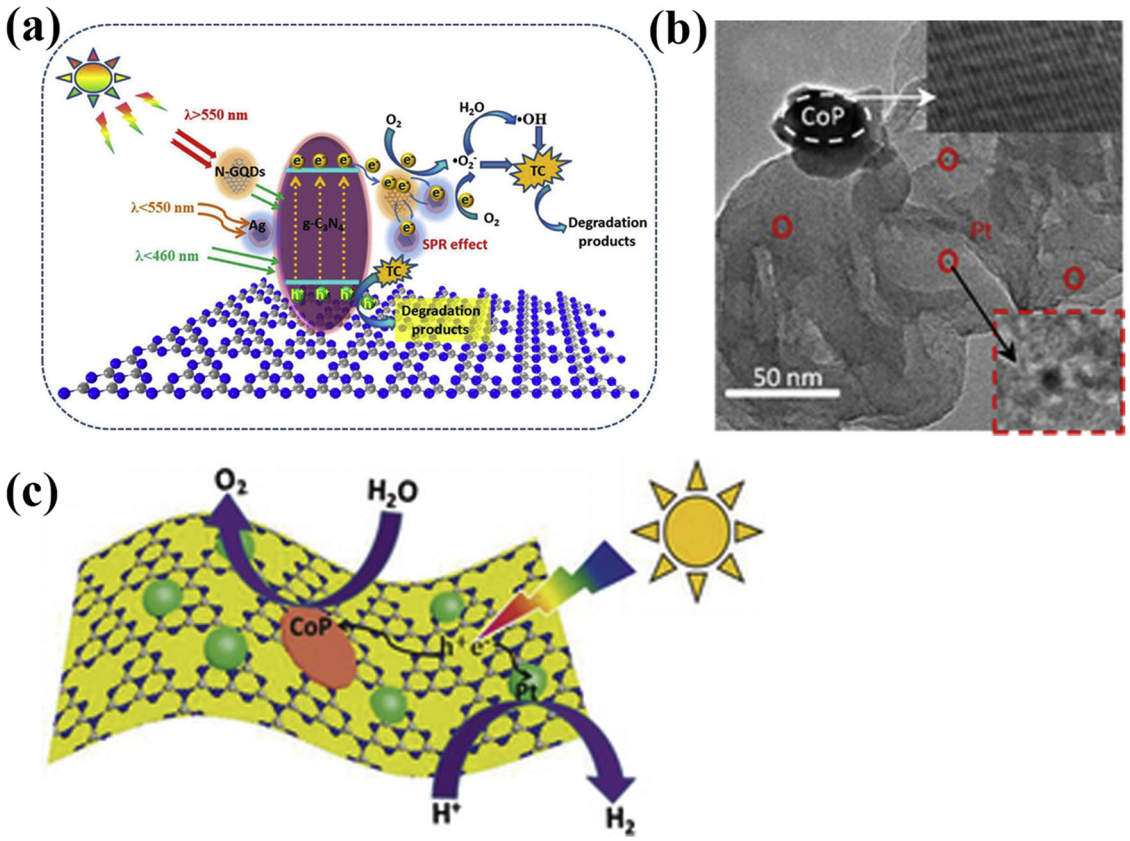

Fig. 10. (a) The proposed photocatalytic reaction mechanism and charge-transfer pathway over Ag/N-GQDs/g-C_3N_4 nanocomposites toward TC degradation under full-spectrum light irradiation. Reprinted with permission from Ref. [191]. Copyright 2017 American Chemical Society. **(b)** TEM image of the optimum Pt-CoP/g-C_3N_4. **(c)** Mechanism of Pt and CoP co-doped CNNs for photocatalytic water splitting. Reprinted with permission from Ref. [192]. Copyright 2017 John Wiley & Sons, Inc.

systems emphasize on the interaction of each kind of nanoparticle with CNNs. They are usually fabricated by loading two kinds of 0D nanomaterials onto CNNs successively. For example, Ramakrishna et al. fabricated Ag NPs-CDots/CNNs through depositing CDots onto CNNs by impregnation-hydrothermal method first to obtain CDots/CNNs and then depositing Ag NPs onto CDots/CNNs [190]. CNNs decorated with 2 wt% CDots and 1 wt% Ag NPs showed the highest degradation performance to MO and p-nitrophenol. In this system, the electrons storing ability of CDots and SPR effect of Ag NPs were combined and realized enhanced photocatalytic activity. At the same time, they demonstrated that excess amount of CDots and Ag NPs would decrease the photocatalytic performance because their cover on CNNs limited the light absorption and they could serve as charge carrier recombination sites to some extent. The similar study was conducted by Wang et al. to fabricate Pt NPs-CDots/CNNs and it exhibited excellent activity for the same mechanism [108]. Deng et al. fabricated ternary Ag-nitrogen doped graphene QDs (N-GQDs)/g-C_3N_4 nanocomposites with enhanced light response even for near-infrared light (Fig. 10a) [191]. In this system, CNNs serve as the reaction matrix and support for N-GQDs and Ag NPs to inhibit their agglomeration. It can absorb the UV and visible light with wavelengths less than 460 nm and generate photoexcited electrons and holes. Ag NPs are the contributor for the light with the wavelengths shorter than 550 nm due to their SPR effect. N-GQDs are dominant under light with wavelengths longer than 550 nm for their up-conversion effect to convert longer wavelengths to shorter wavelengths and it can effectively improve both the charge separation and light utilization. Furthermore, the SPR effect of Ag NPs contributes to more visible light absorption, which further promotes the light harvesting capacity of N-GQDs. So Ag-*N*-GQDs/g-C_3N_4 presents enhanced performance under full-spectrum light. Also, results demonstrate the 0.5 wt% N-GQDs and 2.0 wt% Ag NPs co-doped CNNs exhibit the highest photocatalytic activity for TC degradation and it shows the same tendency as the former study that excess amount of N-GQDs and Ag NPs would decrease the photocatalytic performance. Therefore, in this kind system, a suitable balance should be found in the amount of the deposited 0D nanomaterials to realize the optimal cooperation during the photocatalytic process. Innovatively, Pan et al. introduced Pt NPs as reductive co-catalysts and CoP NPs as oxidative co-catalysts onto CNNs and this strategy make up the inadequate water oxidation ability of the Pt NPs/CNNs system and realized overall water splitting [192]. The TEM of optimum Pt-CoP/CNNs is exhibited in Fig. 10b, which demonstrates the relative well-dispersion of Pt NPs on CNNs. Fig. 10c depicts the mechanism during the photocatalytic process. Pt NPs on CNNs act as electron traps and provide proton reduction sites for H_2 production while CoP NPs act as O_2 evolution sites, where photoinduced holes are consumed for water oxidation. At the same time, better performance of Pt-CoP/CNNs was found than both CNNs loaded with Pt and CNNs loaded with CoP because Pt and CoP NPs play a synergistic role to realize efficient charge separation and dual co-catalysts contribute to larger number of active sites and enhancing reaction kinetics. So besides the amount of loaded nanoparticles, mutual complement in the function of them should better be taken into consideration for more excellent performance in this kind of system.

The second kind of system is binary nanoparticle decorated CNNs. Compared to the first kind of system, two components in binary nanoparticle also show intimate interaction in this kind of system. They are usually fabricated by preparing binary nanoparticles first and then depositing them on CNNs. Zhang et al. synthesized Ag@AgCl/g-C_3N_4 plasmonic photocatalyst by a rational in situ ion exchange approach between exfoliated 2D CNNs and $AgNO_3$ and it showed excellent

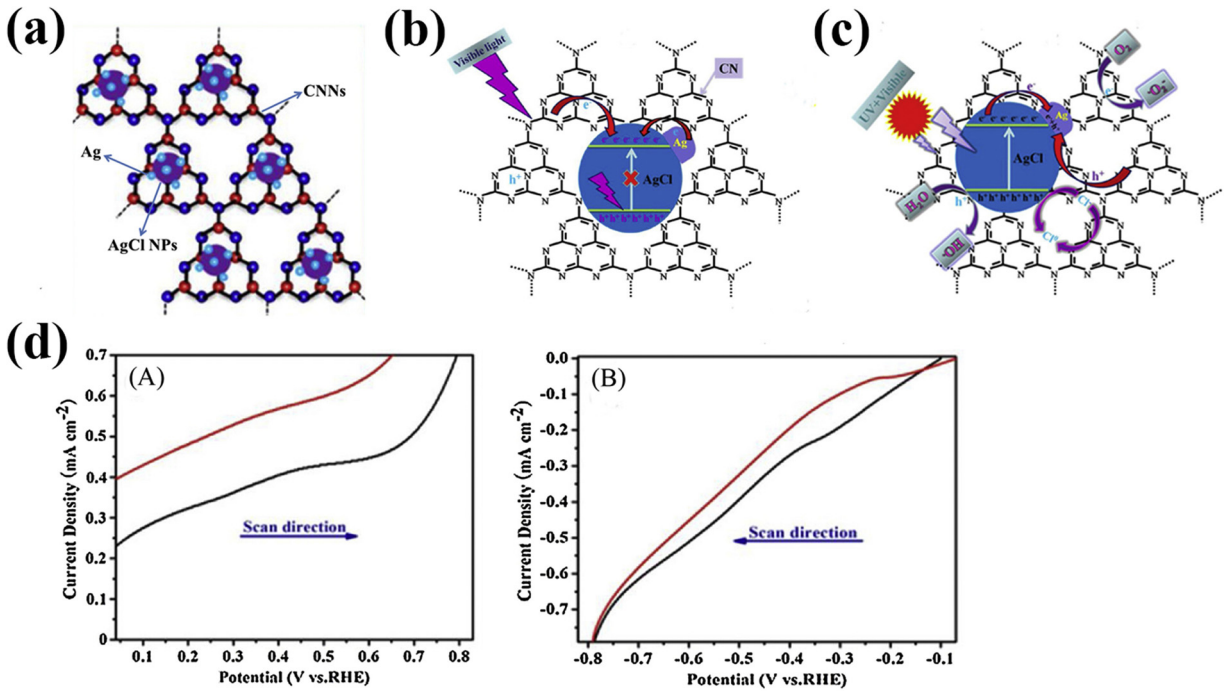

Fig. 11. (a) Schematic structure of Ag@AgCl/CNNs. **(b)** Charge-transfer pathway of Ag@AgCl/CNNs under visible light. **(c)** Charge-transfer pathway of Ag@AgCl/CNNs under the full arc irradiation. **(d)** Anode (A) and cathodic (B) polarization curves of CN and Ag@AgCl/CN-2 under full arc irradiation. Reprinted with permission from Ref. [196].Copyright 2017 Elsevier.

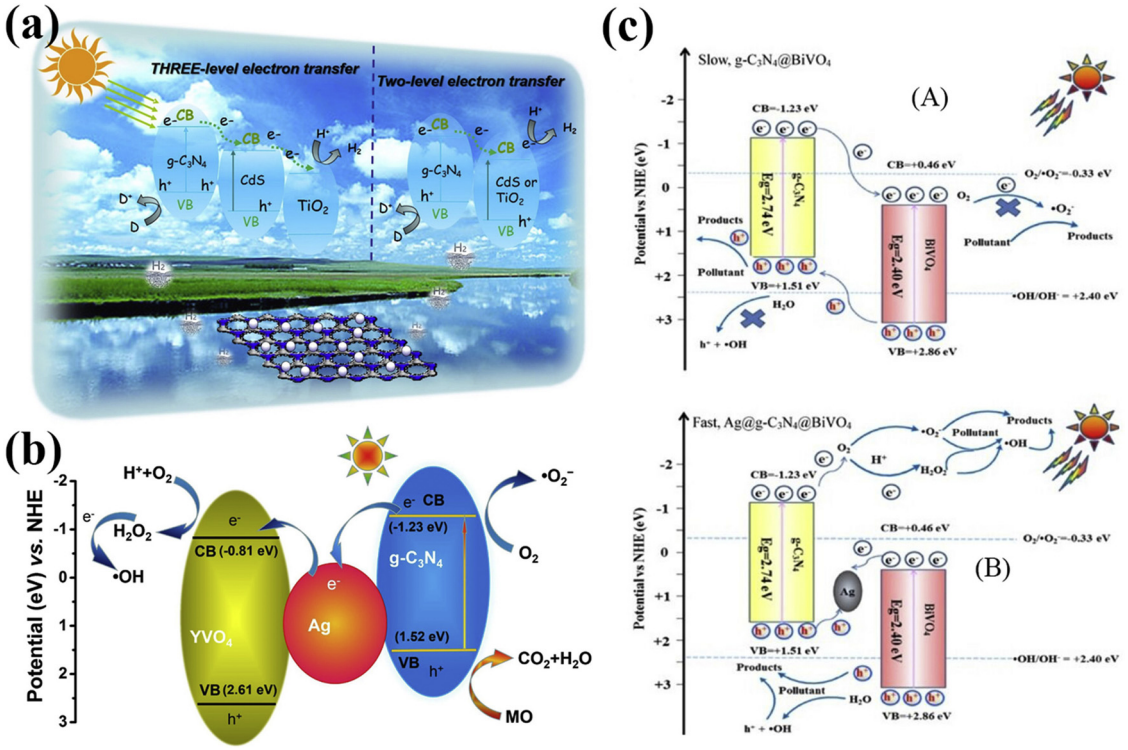

Fig. 12. (a) Compare on the mechanisms of ternary composite CdS-TiO_2/CNNs and binary composite CdS or TiO_2/CNNs for H_2 evolution under visible light. Reprinted with permission from Ref. [197]. Copyright 2017 Elsevier. **(b)** Transfer and separation of charge carrier in the photodegradation of MO by YVO_4/CNNs/Ag. Reprinted with permission from Ref. [198]. Copyright 2017 Elsevier. **(c)** Compare on the charge-transfer pathway of photogenerated electron-hole pairs in binary composite g-C_3N_4@$BiVO_4$ (A) and ternary composite Ag@g-C_3N_4@$BiVO_4$ (B) under visible light irradiation. Reprinted with permission from Ref. [199]. Copyright 2017 Elsevier.

performance for the degradation of RhB under visible light [193]. The significant enhancement in the performance is attributed to the interaction among Ag NPs, AgCl and CNNs. The nanostructure of Ag@AgCl/g-C_3N_4 is illustrated in Fig. 11a. For the Ag@AgCl NPs in Ag@AgCl/g-C_3N_4, improved visible light absorption is achieved for the strong SPR of Ag NPs and the excited electrons on the surface of them are forced away from the interfaces due to the polarization field around AgCl, which prevent the photoreduction of Ag^+ to Ag. Also more electron-hole pairs can be generated by the interaction between the plasmonic Ag clusters and the Cl^- [194]. For the system of AgCl/CN in Ag@AgCl/CN, strong heterojunctions are formed on the interfaces between CNNs and AgCl due to their suitable band gap, which promote the separation and transfer of photogenerated electron-hole pairs. What's more, the Ag@AgCl nanoislands on CNNs provide more active centers by fully exposing the adjacent area of island-sheet interfaces to the pollutants. The charge-transfer pathway is illustrated in Fig. 11b. CNNs can be excited under visible light while AgCl cannot for its wider bandgap. Electrons in CB of CNNs readily injected into the CB of AgCl for its more negative potential than AgCl. At the same time, the excited electrons on the surface of Ag NPs quickly transfer to the CB of AgCl due to the enhanced local inner electromagnetic field and high visible-light absorption capability induced by SPR of Ag NPs. Then separation of photoinduced charge carrier is realized for enhancing the photocatalytic activity. Similar work has been done by Yao et al. for methyl blue degradation [195]. Besides, Li et al. further studied the photocatalytic mechanism of Ag@AgCl QDs/g-C_3N_4 nanoplates under the full arc irradiation (UV and visible light) [196]. Comparing the two conditions, they found that AgCl served as electron acceptor under visible light but electron donor under the full arc irradiation. The charge transition ways of the latter condition are showed in Fig. 11**c**. A Z-scheme system is constructed under the full arc irradiation according to their analysis of Mott-Schottky plots and polarization (anode and cathodic) curves of CN and Ag@AgCl/CN-2 (Fig. 11d). The excited electrons in the CB of AgCl and holes in the VB of CNNs can concurrently transfer to the surface of Ag NPs and contribute to the enrichment of electrons and holes in the CB of CNNs and VB of AgCl, respectively. The different band potentials mean that the electrons and holes show higher redox ability than those under visible light. Jiang et al. synthesized CdS-TiO_2 nanodots and successfully deposited them on 2D CNNs via an epitaxial growth process [197]. This system exhibited enhanced H_2 evolution activity under visible light for the information of ternary heterojunction in the system. As illustrated in Fig. 12a, for the CB potential negativity as follows: g-C_3N_4 > CdS > TiO_2, photoexcited electrons transfer from CB of g-C_3N_4 to CB of CdS and then to CB of TiO_2. The long-distance electron transport of the three-level electron transfer system contributes to more efficient charge carrier separation compared to two-level electron transfer. And CNNs as support also limit the nanoparticles aggregation and facilitate the effective transportation of products and photo-induced carriers. Therefore, this kind system focuses more on the heterojunction formation between different components to realize efficient separation of photoinduced electron-hole pairs.

The third kind of system is metal nanoparticles mediated heterojunction. These systems emphasize on the role of metal nanoparticles as mediator. They are usually fabricated by photodeposition of metal nanoparticles onto CNNs based binary heterostructure. The performance of binary system is enhanced through introducing metal atoms to serve as electron-shuttle mediators and facilitate the charge transfer during the photocatalytic process. Take Ag atoms for example, Gao et al. successfully fabricated YVO_4/CNNs/Ag and they showed outstanding performance in the degradation of MO compared to g-C_3N_4 [198]. As shown in Fig. 12b, the photogenerated electrons transfer from CB of g-C_3N_4 to CB of YVO_4 due to the different potentials between them. And the introduced Ag NPs act as an electrons transportation bridge to facilitate the efficient separation of charge carrier and enhance the visible-light absorption significantly for their SPR effect. Hence enhanced performance was achieved in this Ag atoms mediated ternary system. Chen et al. designed Ag@CNNs@$BiVO_4$ ternary photocatalytic system and realized higher photocatalytic activity for TC degradation than CNNs@$BiVO_4$ binary system [199]. The diversities between them are illustrated in Fig. 12c. In the binary composite $BiVO_4$/CNNs, a typical type II heterojunction is formed between CNNs and $BiVO_4$ but the enriched electrons in the CB of $BiVO_4$ and holes in the VB of CNNs could not produce $^{\cdot}OH$ and $^{\cdot}O_2^-$ for their low redox potentials. However, with the introduction of Ag NPs onto CNNs@$BiVO_4$ by photodeposition, the charge carrier transition ways are changed rather than be promoted and this system realizes the conversion from type II photocatalyst to Z-scheme photocatalyst. Electrons are excited from CB to VB in both CNNs and $BiVO_4$. The photogenerated electrons in the CB of $BiVO_4$ transfer to Ag NPs due to the more negative CB potentials of $BiVO_4$ than that of Ag NPs. The photoinduced holes from CNNs transfer to Ag NPs due to the more positive VB potentials of CNNs than that of Ag NPs. The electrons and holes recombine in Ag NPs and finally contribute to the enrichment of electrons and holes in the CB of CNNs and VB of $BiVO_4$ respectively, which possess higher redox ability compared to type II system. Therefore, in these systems the match of the semiconductor band potentials is primary and metal atoms serve as mediator to promote the charge carrier transfer. Also, CNNs/Ag/Ag_3VO_4 [200], CNNs/Ag/Ag_3PO_4 [163,201] Ag/g-C3N4/NaTaO3 [202] and Au/CNNS/$W_{18}O_{49}$ [203] were fabricated with similar mechanism and presented excellent performance for organic pollutants degradation, water oxidation and chromium (VI) reduction.

From the studies presented above, in the more complex system, the 0D form of carbon, metal and other semiconductors facilitate their dispersion on the surface of CNNs and enhance their contraction with each other. At the same time, the combination of different semiconductor nanoparticles realizes the multi-level charge carrier transition for better electron-hole pairs separation. Metal atoms and carbon nanodots usually play as promoting factors for charge carrier transition and visible light harvesting [109,204,205]. So their cooperation realizes further improvement of the photocatalyst performance.

5. Conclusions and perspectives

In summary, 2D CNNs exhibit increasing applications in the design of photocatalyst due to their excellent physical properties including high specific surface, more surface active sites, superior electron mobility and good dispersion for guest materials. Additionally, 2D CNNs can act as stabilizer to enhance the durability and stability of the loaded materials. Therefore, the position of CNNs becomes more prominent with the increasing tendency to control the morphology of photocatalyst in their fabrication process. 0D nanomaterials, like carbon nanodots, metal atoms, semiconductor nanoparticles, are widely used as ingredients for improving performance of the decorated materials. So 0D/2D photocatalyst based on the combination of CNNs and 0D nanomaterials obtain a system with further enhanced photocatalytic capacity. However, it is worth noting that the performance of 0D nanomaterials/CNNs systems associates strongly with the characters of their components. Thus more efforts should be devoted to control the physical properties of CNNs and the loaded 0D nanomaterials and make a proper design for optimum photocatalytic activity. Herein, several aspects of 2D CNNs as support for 0D nanomaterials in the photocatalytic field deserve further efforts.

(1) The photocatalytic properties like thickness, size, surface composition of CNNs, which are related to their preparation strategies closely, affect their photocatalytic activity and combination with 0D nanomaterials a lot. But there are few quantitative studies about the influence of CNNs thickness and size on 0D nanomaterials/CNNs system performance and few qualitative studies about the influence of the surface composition of CNNs prepared by different precursors and methods on their interaction with 0D nanomaterials.

(2) Recently the stability of C_3N_4 in the photocatalytic applications catches more attention. It was found that $^{\cdot}OH$ generated during the photocatalytic process could tear the heptazine unit directly from C_3N_4 to form cyameluric acid and further release nitrates into the aqueous environment [206]. So as low dimensional morphology of C_3N_4, specific studies need to be conducted on the stability of CNNs with different thickness and 0D materials/CNNs systems in the photocatalytic applications.
(3) Applications of 0D nanomaterials/CNNs systems demand massive production of high-quality CNNs with controllable layers, sizes and compositions. Therefore more effective strategies need to be found to prepare CNNs in rapid, economic and energy-efficient ways. At the same time, more importance should be attached to the development of new-type 2D nanomaterials and their combination with 0D materials.
(4) Summarizing from the studies above, the sizes and distribution of 0D nanomaterials are two crucial factors in the photocatalytic activity of this system. Therefore more efficient strategies should be taken to control the dispersion of 0D nanomaterials on the surface of CNNs. Recently single-atom photocatalysts have been designed by embedding noble metals which were downsized to even single atoms into supported catalysts. This strategy provides an effective way to maximize the atom efficiency and improve the photocatalytic performance of the decorated materials [207–209]. So it is worth looking forward to the fabrication of single atoms photocatalyst based on CNNs for further improved activity.
(5) Novel materials like metal organic framework have been used to combine with g-C_3N_4 recently and show great potential in photocatalyst fabrication. But few studies were conducted to load metal organic framework nanoparticles on CNNs [210,211]. This is a promising field worth exploration. Also, semiconductor quantum dots/CNNs show great potential in the fabrication of CNNs based photocatalyst with excellent capacity. More methods need to be explored to realize the better deposition of quantum dots on the surface of CNNs.
(6) Great progress has been made in the combination of noble metal atoms and CNNs for photocatalytic applications. But the participation of noble metals will cause higher preparation cost and environment pollution to some extent [212–216]. Now few non-noble metals have been combined with CNNs like bismuth [217], zero-valent iron [218–222] show excellent performance in the photocatalytic field for pollutants treatment. Therefore more non-noble metals/CNNs systems can be explored for enhanced photocatalytic activity of CNNs.
(7) Carbon nanodots and noble metal atoms can facilitate the transfer of charge carrier in the photocatalytic system. Therefore more complex systems can be designed by using them as mediators to realize efficient charge transition or even different charge-transfer pathways for higher photocatalytic activity.

Acknowledgements

This review supported by the Program for the National Natural Science Foundation of China (51579098, 51779090, 51709101, 51278176, 51408206, 51521006), the National Program for Support of Top-Notch Young Professionals of China (2014), Hunan Provincial Science and Technology Plan Project (No.2016RS3026), and the Program for Changjiang Scholars and Innovative Research Team in University (IRT-13R17).

References

[1] X. Guo, Z. Peng, D. Huang, P. Xu, G. Zeng, S. Zhou, X. Gong, M. Cheng, R. Deng, H. Yi, H. Luo, X. Yan, T. Li, Biotransformation of cadmium-sulfamethazine combined pollutant in aqueous environments: phanerochaete chrysosporium bring cautious optimism, Chem. Eng. J. 347 (2018) 74–83.
[2] W. Xue, Z. Peng, D. Huang, G. Zeng, J. Wan, R. Xu, M. Cheng, C. Zhang, D. Jiang, Z. Hu, Nanoremediation of cadmium contaminated river sediments: microbial response and organic carbon changes, J. Hazard. Mater. 359 (2018) 290–299.
[3] D. Huang, X. Qin, P. Xu, G. Zeng, R. Wang, J. Wan, X. Gong, W. Xue, Composting of 4-nonylphenol-comtaminated river sediment with inocula of Phanerochaete chrysosporium, Bioresour. Technol. Rep. 221 (2016) 47–54.
[4] R. Wang, D. Huang, Y. Liu, C. Zhang, C. Lai, G. Zeng, M. Cheng, X. Gong, J. Wan, H. Luo, Investigating the adsorption behavior and the relative distribution of Cd^{2+} sorption mechanisms on biochars by different feedstock, Bioresour. Technol. Rep. 261 (2018) 265–271.
[5] D. Huang, Z. Tang, Z. Peng, C. Lai, G. Zeng, C. Zhang, P. Xu, M. Cheng, J. Wan, R. Wang, Fabrication of water-compatible molecularly imprinted polymer based on β-cyclodextrin modified magnetic chitosan and its application for selective removal of bisphenol A from aqueous solution, J. Taiwan. Inst. Chem. E. 77 (2017) 113–121.
[6] N. Zhang, C. Han, Y.J. Xu, J.J. Foley, D. Zhang, J. Codrington, S.K. Gray, Y. Sun, Near-field dielectric scattering promotes optical absorption by platinum nanoparticles, Nat. Photonics 10 (2016) 473–482.
[7] Q. Li, Y. Liu, S. Guo, H. Zhou, Solar energy storage in the rechargeable batteries, Nano Today 16 (2017) 46–60.
[8] N.S. Lewis, Research opportunities to advance solar energy utilization, Science 351 (2016) 6271.
[9] D. Huang, X. Wang, C. Zhang, G. Zeng, Z. Peng, J. Zhou, M. Cheng, R. Wang, Z. Hu, X. Qin, Sorptive removal of ionizable antibiotic sulfamethazine from aqueous solution by graphene oxide-coated biochar nanocomposites: influencing factors and mechanism, Chemosphere 186 (2017) 414–421.
[10] D. Huang, X. Guo, Z. Peng, G. Zeng, P. Xu, X. Gong, R. Deng, W. Xue, R. Wang, H. Yi, C. Liu, White rot fungi and advanced combined biotechnology with nanomaterials: promising tools for endocrine-disrupting compounds biotransformation, Crit. Rev. Biotechnol. (2017) 1–19.
[11] X. Gong, D. Huang, Y. Liu, Z. Peng, G. Zeng, P. Xu, M. Cheng, R. Wang, J. Wan, Remediation of contaminated soils by biotechnology with nanomaterials: bio-behavior, applications, and perspectives, Crit. Rev. Biotechnol. 38 (2018) 455–468.
[12] D. Huang, Y. Wang, C. Zhang, G. Zeng, C. Lai, J. Wan, L. Qin, Y. Zeng, Influence of morphological and chemical features of biochar on hydrogen peroxide activation: implications on sulfamethazine degradation, RSC Adv. 6 (2016) 73186–73196.
[13] D. Huang, R. Wang, Y. Liu, G. Zeng, C. Lai, P. Xu, B. Lu, J. Xu, C. Wang, C. Huang, Application of molecularly imprinted polymers in wastewater treatment: a review, Environ. Sci. Pollut. Res. 22 (2014) 963–977.
[14] A. Fujishima, K. Honda, Electrochemical photolysis of water at a semiconductor electrode, Nature 238 (1972) 37–38.
[15] C. Zhou, C. Lai, C. Zhang, G. Zeng, D. Huang, M. Cheng, L. Hu, W. Xiong, M. Chen, J. Wang, Y. Yang, L. Jiang, Semiconductor/boron nitride composites: synthesis, properties, and photocatalysis applications, Appl. Catal. B Environ. 238 (2018) 6–18.
[16] M. Zhu, Y. Osakada, S. Kim, M. Fujitsuka, T. Majima, Black phosphorus: a promising two dimensional visible and near-infrared-activated photocatalyst for hydrogen evolution, Appl. Catal. B Environ. 217 (2017) 285–292.
[17] X. Bai, C. Sun, D. Liu, X. Luo, D. Li, J. Wang, N. Wang, X. Chang, R. Zong, Y. Zhu, Photocatalytic degradation of deoxynivalenol using graphene/ZnO hybrids in aqueous suspension, Appl. Catal. B Environ. 204 (2017) 11–20.
[18] Y. Zhu, Y. Wang, Q. Ling, Y. Zhu, Enhancement of full-spectrum photocatalytic activity over $BiPO_4/Bi_2WO_6$ composites, Appl. Catal. B Environ. 200 (2017) 222–229.
[19] O.A. Carrasco-Jaim, O. Ceballos-Sanchez, L.M. Torres-Martínez, E. Moctezuma, C. Gómez-Solís, Synthesis and characterization of PbS/ZnO thin film for photocatalytic hydrogen production, J. Photochem. Photobiol. A Chem. 347 (2017) 98–104.
[20] L. Bi, X. Gao, L. Zhang, D. Wang, X. Zou, T. Xie, The enhanced photocatalytic hydrogen evolution of NiCoP/g-C_3N_4 with the improved separation efficiency and charge transfer efficiency, ChemSusChem. 11 (2018).
[21] M.H. Alhaji, K. Sanaullah, A. Khan, A. Hamza, A. Muhammad, S.I. Mustapha, A.R.H. Rigit, S.A. Bhawani, Erratum to: recent developments in immobilizing titanium dioxide on supports for degradation of organic pollutants in wastewater-A review, Int. J. Environ. Sci. Technol. 14 (2017) 2053.
[22] X. Ma, W. Ma, D. Jiang, D. Li, S. Meng, M. Chen, Construction of novel $WO_3/SnNb_2O_6$ hybrid nanosheet heterojunctions as efficient Z-scheme photocatalysts for pollutant degradation, J. Colloid Interface Sci. 506 (2017) 93–101.
[23] C. Zhou, C. Lai, P. Xu, G. Zeng, D. Huang, C. Zhang, M. Cheng, L. Hu, J. Wan, Y. Liu, W. Xiong, Y. Deng, M. Wen, In situ grown $AgI/Bi_{12}O_{17}Cl_2$ heterojunction photocatalysts for visible light degradation of sulfamethazine: efficiency, pathway, and mechanism, ACS Sustain. Chem. Eng. 6 (2018) 4174–4184.
[24] Y. Zhang, L. Li, Q. Han, L. Tang, X. Chen, J. Hu, Z. Li, Y. Zhou, J. Liu, Z. Zou, Bi_2MoO_6 nanostrip networks for enhanced visible-light photocatalytic reduction of CO_2 to CH_4, ChemPhysChem (2017) 1–6.
[25] Z. Sun, J.M.T.A. Fischer, Q. Li, J. Hu, Q. Tang, H. Wang, Z. Wu, M. Hankel, D.J. Searles, L. Wang, Enhanced CO_2 photocatalytic reduction on alkali-decorated graphitic carbon nitride, Appl. Catal. B Environ. 216 (2017) 146–155.
[26] Q. Zhou, S. Ma, S. Zhan, Superior photocatalytic disinfection effect of Ag-3D ordered mesoporous CeO_2 under visible light, Appl. Catal. B Environ. 224 (2018) 27–37.
[27] X. Wang, K. Maeda, A. Thomas, K. Takanabe, G. Xin, J.M. Carlsson, K. Domen, M. Antonietti, A metal-free polymeric photocatalyst for hydrogen production from water under visible light, Nat. Mater. 8 (2009) 76–80.
[28] G. Mamba, A.K. Mishra, Graphitic carbon nitride (g-C_3N_4) nanocomposites: a new and exciting generation of visible light driven photocatalysts for environmental

pollution remediation, Appl. Catal. B Environ. 198 (2016) 347–377.
[29] Y. Zhang, T. Mori, L. Niu, J. Ye, Non-covalent doping of graphitic carbon nitride polymer with graphene: controlled electronic structure and enhanced optoelectronic conversion, Energy Environ. Sci. 4 (2011) 4517.
[30] Y. Hong, C. Li, D. Li, Z. Fang, B. Luo, X. Yan, H. Shen, B. Mao, W. Shi, Precisely tunable thickness of graphitic carbon nitride nanosheets for visible-light-driven photocatalytic hydrogen evolution, Nanoscale 9 (2017) 14103–14110.
[31] S. Guo, Y. Tang, Y. Xie, C. Tian, Q. Feng, W. Zhou, B. Jiang, P-doped tubular g-C_3N_4 with surface carbon defects: universal synthesis and enhanced visible-light photocatalytic hydrogen production, Appl. Catal. B Environ. 218 (2017) 664–671.
[32] C. Zhou, C. Lai, D. Huang, G. Zeng, C. Zhang, M. Cheng, L. Hu, J. Wan, W. Xiong, M. Wen, X. Wen, L. Qin, Highly porous carbon nitride by supramolecular preassembly of monomers for photocatalytic removal of sulfamethazine under visible light driven, Appl. Catal. B Environ. 220 (2018) 202–210.
[33] J. Wang, Z. Yang, X. Gao, W. Yao, W. Wei, X. Chen, R. Zong, Y. Zhu, Core-shell g-C_3N_4@ZnO composites as photoanodes with double synergistic effects for enhanced visible-light photoelectrocatalytic activities, Appl. Catal. B Environ. 217 (2017) 169–180.
[34] H. Wang, X. Yuan, H. Wang, X. Chen, Z. Wu, L. Jiang, W. Xiong, G. Zeng, Facile synthesis of Sb_2S_3/ultrathin g-C_3N_4 sheets heterostructures embedded with g-C_3N_4 quantum dots with enhanced NIR-light photocatalytic performance, Appl. Catal. B Environ. 193 (2016) 36–46.
[35] Z. Huang, F. Li, B. Chen, G. Yuan, Porous and low-defected graphitic carbon nitride nanotubes for efficient hydrogen evolution under visible light irradiation, RSC Adv. 5 (2015) 102700–102706.
[36] M. Tahir, C. Cao, N. Mahmood, F.K. Butt, A. Mahmood, F. Idrees, S. Hussain, M. Tanveer, Z. Ali, I. Aslam, Multifunctional g-C_3N_4 nanofibers: a template-free fabrication and enhanced optical, electrochemical, and photocatalyst properties, ACS Appl. Mater. Interfaces 6 (2014) 1258–1265.
[37] X. Bai, L. Wang, R. Zong, Y. Zhu, Photocatalytic activity enhanced via g-C_3N_4 nanoplates to nanorods, J. Phys. Chem. C. 117 (2013) 9952–9961.
[38] J. Zhang, Y. Wang, J. Jin, J. Zhang, Z. Lin, F. Huang, J. Yu, Efficient visible-light photocatalytic hydrogen evolution and enhanced photostability of core/shell CdS/g-C_3N_4 nanowires, ACS Appl. Mater. Interfaces 5 (2013) 10317–10324.
[39] Y. Yang, L. Geng, Y. Guo, J. Meng, Y. Guo, Easy dispersion and excellent visible-light photocatalytic activity of the ultrathin urea-derived g-C_3N_4 nanosheets, Appl. Surf. Sci. 425 (2017) 535–546.
[40] C. Hu, Y.-C. Chu, M.-S. Wang, X.-H. Wu, Rapid synthesis of g-C_3N_4 spheres using microwave-assisted solvothermal method for enhanced photocatalytic activity, J. Photochem. Photobiol. A Chem. 348 (2017) 8–17.
[41] D. Zheng, C. Huang, X. Wang, Post-annealing reinforced hollow carbon nitride nanospheres for hydrogen photosynthesis, Nanoscale 7 (2015) 465–470.
[42] P. Niu, L. Zhang, G. Liu, H.M. Cheng, Graphene-like carbon nitride nanosheets for improved photocatalytic activities, Adv. Funct. Mater. 22 (2012) 4763–4770.
[43] L. Jiang, X. Yuan, Y. Pan, J. Liang, G. Zeng, Z. Wu, H. Wang, Doping of graphitic carbon nitride for photocatalysis: a reveiw, Appl. Catal. B Environ. 217 (2017) 388–406.
[44] D. Masih, Y. Ma, S. Rohani, Graphitic C_3N_4 based noble-metal-free photocatalyst systems: a review, Appl. Catal. B Environ. 206 (2017) 556–588.
[45] J. Zhang, Y. Chen, X. Wang, Two-dimensional covalent carbon nitride nanosheets: synthesis, functionalization, and applications, Energy Environ. Sci. 8 (2015) 3092–3108.
[46] X. Dong, F. Cheng, Recent development in exfoliated two-dimensional g-C3N_4 nanosheets for photocatalytic applications, J. Mater. Chem. A Mater. Energy Sustain. 3 (2015) 23642–23652.
[47] F. Ding, D. Yang, Z. Tong, Y. Nan, Y. Wang, X. Zou, Z. Jiang, Graphitic carbon nitride-based nanocomposites as visible-light driven photocatalysts for environmental purification, Environ. Sci. Nano 4 (2017) 1455–1469.
[48] Y. Li, W. Cui, L. Liu, R. Zong, W. Yao, Y. Liang, Y. Zhu, Removal of Cr (VI) by 3D TiO_2-graphene hydrogel via adsorption enriched with photocatalytic reduction, Appl. Catal. B Environ. 199 (2016) 412–423.
[49] J. Yang, D. Chen, Y. Zhu, Y. Zhang, Y. Zhu, 3D-3D porous Bi_2WO_6/graphene hydrogel composite with excellent synergistic effect of adsorption-enrichment and photocatalytic degradation, Appl. Catal. B Environ. 205 (2017) 228–237.
[50] Y. Li, J. Zhou, Y. Fan, Y. Ye, B. Tang, Preparation of environment-friendly 3D eggshell membrane-supported anatase TiO_2 as a reusable photocatalyst for degradation of organic dyes, Chem. Phys. Lett. 689 (2017) 142–147.
[51] H.H. El-Maghrabi, A. Barhoum, A.A. Nada, Y.M. Moustafa, S.M. Seliman, A.M. Youssef, M. Bechelany, Synthesis of mesoporous core-shell CdS@TiO_2(0D and 1D) photocatalysts for solar-driven hydrogen fuel production, J. Photochem. Photobiol. A Chem. 351 (2018) 261–270.
[52] D. Jiang, T. Wang, Q. Xu, D. Li, S. Meng, M. Chen, Perovskite oxide ultrathin nanosheets/g-C_3N_4 2D-2D heterojunction photocatalysts with significantly enhanced photocatalytic activity towards the photodegradation of tetracycline, Appl. Catal. B Environ. 201 (2017) 617–628.
[53] Z. Yang, X. Xu, X. Liang, C. Lei, Y. Cui, W. Wu, Y. Yang, Z. Zhang, Z. Lei, Construction of heterostructured MIL-125/Ag/g-C_3N_4 nanocomposite as an efficient bifunctional visible light photocatalyst for the organic oxidation and reduction reactions, Appl. Catal. B Environ. 205 (2017) 42–54.
[54] H. Wang, Y. Liu, M. Li, H. Huang, H.M. Xu, R.J. Hong, H. Shen, Multifunctional TiO_2 nanowires-modified nanoparticles bilayer film for 3D dye-sensitized solar cells, Optoelectron. Adv. Mater. Rapid Commun. 4 (2010) 1166–1169.
[55] Q. Wang, W. Wang, L. Zhong, D. Liu, X. Cao, F. Cui, Oxygen vacancy-rich 2D/2D BiOCl-g-C_3N_4 ultrathin heterostructure nanosheets for enhanced visible-light-driven photocatalytic activity in environmental remediation, Appl. Catal. B Environ. 220 (2018) 290–302.
[56] J. Yan, Y. Fan, J. Lian, Y. Zhao, Y. Xu, J. Gu, Y. Song, H. Xu, H. Li, Kinetics and mechanism of enhanced photocatalytic activity employing ZnS nanospheres/graphene-like C_3N_4, Mol. Catal. 438 (2017) 103–112.
[57] Y. Lei, C. Yang, J. Hou, F. Wang, S. Min, X. Ma, Z. Jin, J. Xu, G. Lu, K.W. Huang, Strongly coupled CdS/graphene quantum dots nanohybrids for highly efficient photocatalytic hydrogen evolution: unraveling the essential roles of graphene quantum dots, Appl. Catal. B Environ. 216 (2017) 59–69.
[58] L. Liu, X. Zhang, L. Yang, L. Ren, D. Wang, J. Ye, Metal nanoparticles induced photocatalysis, Sci. Rev. 4 (2017) 761–780.
[59] W.N. Wang, C.X. Huang, C.Y. Zhang, M.L. Zhao, J. Zhang, H.J. Chen, Z.B. Zha, T. Zhao, H.S. Qian, Controlled synthesis of upconverting nanoparticles/$Zn_xCd_{1-x}S$ yolk-shell nanoparticles for efficient photocatalysis driven by NIR light, Appl. Catal. B Environ. 224 (2018) 854–862.
[60] T.Y. Ma, J.L. Cao, M. Jaroniec, S.Z. Qiao, Interacting carbon nitride and titanium carbide nanosheets for high-performance oxygen evolution, Angew. Chemie-Int. Ed. 55 (2016) 1138–1142.
[61] W.J. Ong, L.L. Tan, Y.H. Ng, S.T. Yong, S.P. Chai, Graphitic carbon nitride (g-C_3N_4)-based photocatalysts for artificial photosynthesis and environmental remediation: are we a step closer to achieving sustainability? Chem. Rev. 116 (2016) 7159–7329.
[62] D. Ghosh, G. Periyasamy, B. Pandey, S.K. Pati, Computational studies on magnetism and the optical properties of transition metal embedded graphitic carbon nitride sheets, J. Mater. Chem. C. 2 (2014) 7943–7951.
[63] I. Nikitskiy, S. Goossens, D. Kufer, T. Lasanta, G. Navickaite, F.H.L. Koppens, G. Konstantatos, Integrating an electrically active colloidal quantum dot photodiode with a graphene phototransistor, Nat. Commun. 7 (2016) 1–8.
[64] Y. Lu, C. Ji, Y. Li, R. Qu, C. Sun, Y. Zhang, Facile one-pot synthesis of C and g-C_3N_4 composites with enhanced photocatalytic activity using hydroxymethylated melamine as carbon source and soft template, Mater. Lett. 211 (2018) 78–81.
[65] X. Liu, F. Pang, M. He, J. Ge, Confined reaction inside nanotubes: new approach to mesoporous g-C_3N_4 photocatalysts, Nano Res. 10 (2017) 3638–3647.
[66] T. Muhmood, M.A. Khan, M. Xia, W. Lei, F. Wang, Y. Ouyang, Enhanced photoelectrochemical, photo-degradation and charge separation ability of graphitic carbon nitride (g-C_3N_4) by self-type metal free heterojunction formation for antibiotic degradation, J. Photochem. Photobiol. A Chem. 348 (2017) 118–124.
[67] J. Oh, J.M. Lee, Y. Yoo, J. Kim, S.J. Hwang, S. Park, New insight of the photocatalytic behaviors of graphitic carbon nitrides for hydrogen evolution and their associations with grain size, porosity, and photophysical properties, Appl. Catal. B Environ. 218 (2017) 349–358.
[68] M. Bellardita, E.I. García-López, G. Marcì, I. Krivtsov, J.R. García, L. Palmisano, Selective photocatalytic oxidation of aromatic alcohols in water by using P-doped g-C_3N_4, Appl. Catal. B Environ. 220 (2018) 222–233.
[69] H. Lin, Y. Liu, J. Deng, S. Xie, X. Zhao, J. Yang, K. Zhang, Z. Han, H. Dai, Graphitic carbon nitride-supported iron oxides: high-performance photocatalysts for the visible-light-driven degradation of 4-nitrophenol, J. Photochem. Photobiol. A Chem. 336 (2017) 105–114.
[70] Y. Li, R. Jin, X. Fang, Y. Yang, M. Yang, X. Liu, Y. Xing, S. Song, In situ loading of Ag_2WO_4 on ultrathin g-C_3N_4 nanosheets with highly enhanced photocatalytic performance, J. Hazard. Mater. 313 (2016) 219–228.
[71] S. Yang, Y. Gong, J. Zhang, L. Zhan, L. Ma, Z. Fang, R. Vajtai, X. Wang, P.M. Ajayan, Exfoliated graphitic carbon nitride nanosheets as efficient catalysts for hydrogen evolution under visible light, Adv. Mater. 25 (2013) 2452–2456.
[72] H. Zhao, H. Yu, X. Quan, S. Chen, Y. Zhang, H. Zhao, H. Wang, Fabrication of atomic single layer graphitic-C_3N_4 and its high performance of photocatalytic disinfection under visible light irradiation, Appl. Catal. B, Environ. 152-153 (2014) 46–50.
[73] J. Liu, J. Huang, D. Dontosova, M. Antonietti, Facile synthesis of carbon nitride micro-/nanoclusters with photocatalytic activity for hydrogen evolution, RSC Adv. 3 (2013) 22988.
[74] Z. Huang, F. Li, B. Chen, G. Yuan, Nanoporous photocatalysts developed through heat-driven stacking of graphitic carbon nitride nanosheets, RSC Adv. 5 (2015) 14027–14033.
[75] M. Wu, J.-M. Yan, X. Tang, M. Zhao, Q. Jiang, Synthesis of potassium-modified graphitic carbon nitride with high photocatalytic activity for hydrogen evolution, ChemSusChem 7 (2014) 2654–2658.
[76] Y. Bu, Z. Chen, T. Xie, W. Li, J.-P. Ao, Fabrication of C_3N_4 ultrathin flakes by mechanical grind method with enhanced photocatalysis and photoelectrochemical performance, RSC Adv. 6 (2016) 47813–47819.
[77] P. Qiu, H. Chen, C. Xu, N. Zhou, F. Jiang, X. Wang, Y. Fu, Fabrication of an exfoliated graphitic carbon nitride as a highly active visible light photocatalyst, J. Mater. Chem. A Mater. Energy Sustain. 3 (2015) 24237–24244.
[78] B. Shen, J. Ding, X. Yan, W. Feng, J. Li, Q. Xue, Influence of different buffer gases on synthesis of few-layered graphene by arc discharge method, Appl. Surf. Sci. 258 (2012) 4523–4531.
[79] J. Zhang, M. Zhang, L. Lin, X. Wang, Sol processing of conjugated carbon nitride powders for thin-film fabrication, Angew. Chemie-Int. Ed. 54 (2015) 6297–6301.
[80] Y. Hong, C. Li, Z. Fang, B. Luo, W. Shi, Rational synthesis of ultrathin graphitic carbon nitride nanosheets for efficient photocatalytic hydrogen evolution, Carbon N.Y. 121 (2017) 463–471.
[81] Q. Liu, X. Wang, Q. Yang, Z. Zhang, X. Fang, A novel route combined precursor-hydrothermal pretreatment with microwave heating for preparing holey g-C_3N_4 nanosheets with high crystalline quality and extended visible light absorption, Appl. Catal. B Environ. 225 (2018) 22–29.
[82] W. Yang, X. Zhang, Y. Xie, Advances and challenges in chemistry of two-dimensional nanosheets, Nano Today 11 (2016) 793–816.
[83] J. Wen, J. Xie, X. Chen, X. Li, A review on g-C_3N_4-based photocatalysts, Appl. Surf.

Sci. 391 (2017) 72–123.
[84] Q. Gu, X. Gong, Q. Jia, J. Liu, Z. Gao, X. Wang, J. Long, C. Xue, Compact carbon nitride based copolymer films with controllable thickness for photoelectrochemical water splitting, J. Mater. Chem. A 5 (2017) 19062–19071.
[85] Z. Sun, H. Wang, Z. Wu, L. Wang, G-C_3N_4 based composite photocatalysts for photocatalytic CO_2 reduction, Catal. Today 300 (2017) 160–172.
[86] L. Jiang, X. Yuan, G. Zeng, Z. Wu, J. Liang, X. Chen, L. Leng, H. Wang, H. Wang, Metal-free efficient photocatalyst for stable visible-light photocatalytic degradation of refractory pollutant, Appl. Catal. B Environ. 221 (2018) 715–725.
[87] X. Zhang, Y. Xie, Recent advances in free-standing two-dimensional crystals with atomic thickness: design, assembly and transfer strategies, Chem. Soc. Rev. 42 (2013) 8187.
[88] X.H. Song, L. Feng, S.L. Deng, S.Y. Xie, L.S. Zheng, Simultaneous exfoliation and modification of graphitic carbon nitride nanosheets, Adv. Mater. Interfaces 4 (2017) 1700339.
[89] D. Chen, K. Wang, D. Xiang, R. Zong, W. Yao, Y. Zhu, Significantly enhancement of photocatalytic performances via core-shell structure of ZnO@mpg-C_3N_4, Appl. Catal. B Environ. 147 (2014) 554–561.
[90] J. Zhang, X. Gong, B. Xu, Y. Xia, J. Yin, Z. Liu, Half-metallicity in graphitic C_3N_4 nanoribbons: an *ab initio* study, Phys. Status Solidi 251 (2014) 1386–1392.
[91] J. Tong, L. Zhang, F. Li, M. Li, S. Cao, An efficient top-down approach for the fabrication of large-aspect-ratio g-C_3N_4 nanosheets with enhanced photocatalytic activities, Phys. Chem. Chem. Phys. 17 (2015) 23532–23537.
[92] J. Di, J. Xia, H. Li, Z. Liu, Freestanding atomically-thin two-dimensional materials beyond graphene meeting photocatalysis: opportunities and challenges, Nano Energy 35 (2017) 79–91.
[93] J. Zhang, M. Zhang, C. Yang, X. Wang, Nanospherical carbon nitride frameworks with sharp edges accelerating charge collection and separation at a soft photocatalytic interface, Adv. Mater. 26 (2014) 4121–4126.
[94] Y. Sun, S. Gao, F. Lei, C. Xiao, Y. Xie, Ultrathin two-dimensional inorganic materials: new opportunities for solid state nanochemistry, Acc. Chem. Res. 48 (2015) 3–12.
[95] S. Kumar, A. Kumar, A. Bahuguna, V. Sharma, V. Krishnan, Two-dimensional carbon-based nanocomposites for photocatalytic energy generation and environmental remediation applications, Beilstein J. Nanotechnol. 8 (2017) 1571–1600.
[96] P. Shao, J. Tian, B. Liu, W. Shi, S. Gao, Y. Song, M. Ling, F. Cui, Morphology-tunable ultrafine metal oxide nanostructures uniformly grown on graphene and their applications in the photo-Fenton system, Nanoscale 7 (2015) 14254–14263.
[97] H. Yu, R. Shi, Y. Zhao, G.I.N. Waterhouse, L. Wu, C. Tung, Smart utilization of carbon dots in semiconductor photocatalysis, Adv. Mater. 28 (2016) 9454–9477.
[98] R. Wang, K. Lu, Z. Tang, Y. Xu, Recent progress in carbon quantum dots: synthesis, properties and applications in photocatalysis, J. Mater. Chem. A 5 (2017) 3717–3734.
[99] W.J. Ong, L.K. Putri, Y.C. Tan, L.L. Tan, N. Li, Y.H. Ng, X. Wen, S.P. Chai, Unravelling charge carrier dynamics in protonated g-C_3N_4 interfaced with carbon nanodots as co-catalysts toward enhanced photocatalytic CO_2 reduction: a combined experimental and first-principles DFT study, Nano Res. 10 (2017) 1673–1696.
[100] K. Li, F.Y. Su, W. De Zhang, Modification of g-C_3N_4 nanosheets by carbon quantum dots for highly efficient photocatalytic generation of hydrogen, Appl. Surf. Sci. 375 (2016) 110–117.
[101] Y. Wang, X. Liu, J. Liu, B. Han, X. Hu, F. Yang, Z. Xu, Y. Li, S. Jia, Z. Li, Y. Zhao, Carbon quantum dot implanted graphite carbon nitride nanotubes: excellent charge separation and enhanced photocatalytic hydrogen evolution, Angew. Chemie-Int. Ed. 57 (2018) 5765–5771.
[102] Y. Hong, Y. Meng, G. Zhang, B. Yin, Y. Zhao, W. Shi, C. Li, Facile fabrication of stable metal-free CQDs/g-C_3N_4 heterojunctions with efficiently enhanced visible-light photocatalytic activity, Sep. Purif. Technol. 171 (2016) 229–237.
[103] Q. Liu, T. Chen, Y. Guo, Z. Zhang, X. Fang, Ultrathin g-C_3N_4 nanosheets coupled with carbon nanodots as 2D/0D composites for efficient photocatalytic H_2 evolution, Appl. Catal. B Environ. 193 (2016) 248–258.
[104] X. Jian, X. Liu, H. Yang, J. Li, X. Song, H. Dai, Z. Liang, Construction of carbon quantum dots/proton-functionalized graphitic carbon nitride nanocomposite via electrostatic self-assembly strategy and its application, Appl. Surf. Sci. 370 (2016) 514–521.
[105] H. Ming, Z. Ma, Y. Liu, K. Pan, H. Yu, F. Wang, Z. Kang, Large scale electrochemical synthesis of high quality carbon nanodots and their photocatalytic property, Dalton Trans. 41 (2012) 9526–9531.
[106] X. Xia, N. Deng, G. Cui, J. Xie, X. Shi, Y. Zhao, Q. Wang, W. Wang, B. Tang, NIR light induced H_2 evolution by a metal-free photocatalyst, Chem. Commun. 51 (2015) 10899–10902.
[107] H. Zhang, L. Zhao, F. Geng, L. Guo, B. Wan, Y. Yang, Carbon dots decorated graphitic carbon nitride as an efficient metal-free photocatalyst for phenol degradation, Appl. Catal. B, Environ. 180 (2016) 656–662.
[108] X. Wang, J. Cheng, H. Yu, J. Yu, A facile hydrothermal synthesis of carbon dots modified g-C_3N_4 for enhanced photocatalytic H_2-evolution performance, Dalton Trans. 46 (2017) 6417–6424.
[109] Z. Xie, Y. Feng, F. Wang, D. Chen, Q. Zhang, Y. Zeng, Construction of carbon dots modified MoO_3/g-C_3N_4 Z-scheme photocatalyst with enhanced visible-light photocatalytic activity for the degradation of tetracycline, Appl. Catal. B Environ. 229 (2018) 96–104.
[110] C. Xu, Q. Han, Y. Zhao, L. Wang, Y. Li, L. Qu, Sulfur-doped graphitic carbon nitride decorated with graphene quantum dots for an efficient metal-free electrocatalyst, J. Mater. Chem. A 3 (2015) 1841–1846.
[111] J. Liu, Y. Liu, N. Liu, Y. Han, X. Zhang, H. Huang, Y. Lifshitz, S. Lee, J. Zhong, Z. Kang, Metal-free efficient photocatalyst for stable visible water splitting via a two-electron pathway, Science. 347 (2015) 970–974.
[112] G. Gao, Y. Jiao, F. Ma, Y. Jiao, E. Waclawik, A. Du, Carbon nanodot decorated graphitic carbon nitride: new insights into the enhanced photocatalytic water splitting from ab initio studies, Phys. Chem. Chem. Phys. 17 (2015) 31140–31144.
[113] T. Qin, Z. You, H. Wang, Q. Shen, F. Zhang, H. Yang, Preparation and photocatalytic behavior of carbon-nanodots/graphitic carbon nitride composite photocatalyst, J. Electrochem. Soc. 164 (2017) 211–214.
[114] Q. Liu, T. Chen, Y. Guo, Z. Zhang, X. Fang, Grafting Fe (III) species on carbon nanodots/Fe-doped g-C_3N_4 via interfacial charge transfer effect for highly improved photocatalytic performance, Appl. Catal. B Environ. 205 (2017) 173–181.
[115] S. Fang, Y. Xia, K. Lv, Q. Li, J. Sun, M. Li, Effect of carbon-dots modification on the structure and photocatalytic activity of g-C_3N_4, Appl. Catal. B Environ. 185 (2016) 225–232.
[116] J. Feng, G. Liu, S. Yuan, Y. Ma, Influence of functional groups on water splitting in carbon nanodot and graphitic carbon nitride composites: a theoretical mechanism study, Phys. Chem. Chem. Phys. 19 (2017) 4997–5003.
[117] K.L. Kelly, E. Coronado, L.L. Zhao, G.C. Schatz, The optical properties of metal nanoparticles: the influence of size, shape, and dielectric environment, J. Phys. Chem. B 107 (2003) 668–677.
[118] J. Li, S.K. Cushing, J. Bright, F. Meng, T.R. Senty, P. Zheng, A.D. Bristow, N. Wu, Ag@Cu_2O core-shell nanoparticles as visible-light plasmonic photocatalysts, ACS Catal. 3 (2013) 47–51.
[119] D.B. Ingram, P. Christopher, J.L. Bauer, S. Linic, Predictive model for the design of plasmonic metal/semiconductor composite photocatalysts, ACS Catal. 1 (2011) 1441–1447.
[120] Z. Li, J. Wang, K. Zhu, F. Ma, A. Meng, Ag/g-C_3N_4 composite nanosheets: synthesis and enhanced visible photocatalytic activities, Mater. Lett. 145 (2015) 167–170.
[121] J. Jin, Q. Liang, C. Ding, Z. Li, S. Xu, Simultaneous synthesis-immobilization of Ag nanoparticles functionalized 2D g-C_3N_4 nanosheets with improved photocatalytic activity, J. Alloys Compd. 691 (2017) 763–771.
[122] Y. Fu, T. Huang, L. Zhang, J. Zhu, X. Wang, Ag/g-C_3N_4 catalyst with superior catalytic performance for the degradation of dyes: a borohydride-generated superoxide radical approach, Nanoscale. 7 (2015) 13723–13733.
[123] H. Li, Y. Jing, X. Ma, T. Liu, L. Yang, B. Liu, S. Yin, Y. Wei, Y. Wang, Construction of a well-dispersed Ag/graphene-like g-C_3N_4 photocatalyst and enhanced visible light photocatalytic activity, RSC Adv. 7 (2017) 8688–8693.
[124] X. Lü, J. Shen, Z. Wu, J. Wang, J. Xie, Deposition of Ag nanoparticles on g-C_3N_4 nanosheet by N,N-dimethylformamide: soft synthesis and enhanced photocatalytic activity, J. Mater. Res. 29 (2014) 2170–2178.
[125] L. Wang, M. Yu, C. Wu, N. Deng, C. Wang, X. Yao, Synthesis of Ag/g-C_3N_4 composite as highly efficient visible-light photocatalyst for oxidative amidation of aromatic aldehydes, Adv. Synth. Catal. 358 (2016) 2631–2641.
[126] S. Ma, S. Zhan, Y. Jia, Q. Shi, Q. Zhou, Enhanced disinfection application of Ag-modified g-C_3N_4 composite under visible light, Appl. Catal. B Environ. 186 (2016) 77–87.
[127] J. Yi, X. She, Y. Song, H. Xu, P. Zhang, Z. Mo, L. Liu, D. Du, H. Li, A silver on 2D white-C_3N_4 support photocatalyst for mechanistic insights: synergetic utilization of plasmonic effect for solar hydrogen evolution, RSC Adv. 6 (2016).
[128] N. Cheng, J. Tian, Q. Liu, C. Ge, A.H. Qusti, A.M. Asiri, A.O. Al-Youbi, X. Sun, Au-nanoparticle-loaded graphitic carbon nitride nanosheets: green photocatalytic synthesis and application toward the degradation of organic pollutants, ACS Appl. Mater. Interfaces 5 (2013) 6815–6819.
[129] S. Tonda, S. Kumar, V. Shanker, Surface plasmon resonance-induced photocatalysis by Au nanoparticles decorated mesoporous g-C_3N_4 nanosheets under direct sunlight irradiation, Mater. Res. Bull. 75 (2016) 51–58.
[130] G. Nie, P. Li, J.-X. Liang, C. Zhu, Theoretical investigation on the photocatalytic activity of the Au/g-C_3N_4 monolayer, J. Theor. Comput. Chem. 16 (2017) 1750013.
[131] Z. Ni, F. Dong, H. Huang, Y. Zhang, New insights into how Pd nanoparticles influence the photocatalytic oxidation and reduction ability of g-C_3N_4 nanosheets, Catal. Sci. Technol. 6 (2016) 6448–6458.
[132] J. Xue, S. Ma, Y. Zhou, Z. Zhang, M. He, Facile photochemical synthesis of Au/Pt/g-C_3N_4 with plasmon-enhanced photocatalytic activity for antibiotic degradation, ACS Appl. Mater. Interfaces 7 (2015) 9630–9637.
[133] C. Han, Y. Gao, S. Liu, L. Ge, N. Xiao, D. Dai, B. Xu, C. Chen, Facile synthesis of AuPd/g-C_3N_4 nanocomposite: an effective strategy to enhance photocatalytic hydrogen evolution activity, Int. J. Hydrogen Energy (2017) 1–11.
[134] G. Darabdhara, M.R. Das, Bimetallic Au-Pd nanoparticles on 2D supported graphitic carbon nitride and reduced graphene oxide sheets: a comparative photocatalytic degradation study of organic pollutants in water, Chemosphere 197 (2018) 817.
[135] W. Fang, Y. Deng, L. Tang, G. Zeng, Y. Zhou, X. Xie, J. Wang, Y. Wang, J. Wang, Synthesis of Pd/Au bimetallic nanoparticle-loaded ultrathin graphitic carbon nitride nanosheets for highly efficient catalytic reduction of p-nitrophenol, J. Colloid Interface Sci. 490 (2017) 834–843.
[136] S. Liang, Y. Xia, S. Zhu, S. Zheng, Y. He, J. Bi, M. Liu, L. Wu, Au and Pt co-loaded g-C_3N_4 nanosheets for enhanced photocatalytic hydrogen production under visible light irradiation, Appl. Surf. Sci. 358 (2015) 304–312.
[137] C. Han, Y. Lu, J. Zhang, L. Ge, Y. Li, C. Chen, Y. Xin, L. Wu, S. Fang, Novel PtCo alloy nanoparticle decorated 2D g-C3N4 nanosheets with enhanced photocatalytic activity for H_2 evolution under visible light irradiation, J. Mater. Chem. A 3 (2015) 23274–23282.
[138] D. Voiry, H. Shin, K. Loh, M. Chhowalla, Low-dimensional catalysts for hydrogen evolution and CO_2 reduction, Nat. Rev. Chem. 1 (2018) 0105.
[139] S. Tonda, S. Kumar, V. Shanker, In situ growth strategy for highly efficient Ag_2CO_3/g-C_3N_4 hetero/nanojunctions with enhanced photocatalytic activity

under sunlight irradiation, J. Environ. Chem. Eng. 3 (2015) 852–861.
[140] M. Cheng, G. Zeng, D. Huang, C. Lai, P. Xu, C. Zhang, Y. Liu, Hydroxyl radicals based advanced oxidation processes (AOPs) for remediation of soils contaminated with organic compounds: a review, Chem. Eng. J. 284 (2016) 582–598.
[141] W. Jo, T.S. Natarajan, Influence of TiO_2 morphology on the photocatalytic efficiency of direct Z-scheme g-C_3N_4/TiO_2 photocatalysts for isoniazid degradation, Chem. Eng. J. 281 (2015) 549–565.
[142] M.Y. Ye, Z.H. Zhao, Z.F. Hu, L.Q. Liu, H.M. Ji, Z.R. Shen, T.Y. Ma, 0D/2D heterojunctions of vanadate quantum dots/graphitic carbon nitride nanosheets for enhanced visible-light-driven photocatalysis, Angew. Chemie-Int. Ed. 56 (2017) 8407–8411.
[143] S. Zhang, H. Gao, X. Liu, Y. Huang, X. Xu, N.S. Alharbi, T. Hayat, J. Li, Hybrid 0D-2D nanoheterostructures: in situ growth of amorphous silver silicates dots on g-C_3N_4 nanosheets for full-spectrum photocatalysis, ACS Appl. Mater. Interfaces 8 (2016) 35138–35149.
[144] J. Zhang, Z. Ma, Novel β-Ag_2MoO_4/g-C_3N_4 heterojunction catalysts with highly enhanced visible-light-driven photocatalytic activity, RSC Adv. 7 (2017) 2163–2171.
[145] W. Yin, S. Bai, Y. Zhong, Z. Li, Y. Xie, Direct generation of fine Bi2WO_6 nanocrystals on g-C_3N_4 nanosheets for enhanced photocatalytic activity, ChemNanoMat 2 (2016) 732–738.
[146] P. Murugesan, S. Narayanan, M. Manickam, P. Kumar, R. Subbiah, A direct Z-scheme plasmonic AgCl@g-C_3N_4 heterojunction photocatalyst with superior visible light CO_2 reduction in aqueous medium, Appl. Surf. Sci. 450 (2018) 516–526.
[147] W.C. Peng, X.Y. Li, Synthesis of MoS_2/g-C_3N_4 as a solar light-responsive photocatalyst for organic degradation, Catal. Commun. 49 (2014) 63–67.
[148] X. Hao, J. Zhou, Z. Cui, Y. Wang, Y. Wang, Z. Zou, Zn-vacancy mediated electron-hole separation in ZnS/g-C_3N_4 heterojunction for efficient visible-light photocatalytic hydrogen production, Appl. Catal. B Environ. 229 (2018) 41–51.
[149] Y. Lu, D. Chu, M. Zhu, Y. Du, P. Yang, Exfoliated carbon nitride nanosheets decorated with NiS as an efficient noble-metal-free visible-light-driven photocatalyst for hydrogen evolution, Phys. Chem. Chem. Phys. 17 (2015) 17355–17361.
[150] L. Yang, J. Huang, L. Shi, L. Cao, H. Liu, Y. Liu, Y. Li, H. Song, Y. Jie, J. Ye, Sb doped SnO_2-decorated porous g-C_3N_4 nanosheet heterostructures with enhanced photocatalytic activities under visible light irradiation, Appl. Catal. B Environ. 221 (2018) 670–680.
[151] Y. Li, J. Wang, Y. Yang, Y. Zhang, D. He, Q. An, G. Cao, Seed-induced growing various TiO_2 nanostructures on g-C_3N_4 nanosheets with much enhanced photocatalytic activity under visible light, J. Hazard. Mater. 292 (2015) 79–89.
[152] Y. Tan, Z. Shu, J. Zhou, T. Li, W. Wang, Z. Zhao, One-step synthesis of nanostructured g-C_3N_4/TiO_2 composite for highly enhanced visible-light photocatalytic H_2 evolution, Appl. Catal. B Environ. 230 (2018) 260–268.
[153] H. Zhang, W. Tian, L. Zhou, H. Sun, M. Tade, S. Wang, Monodisperse Co_3O_4 quantum dots on porous carbon nitride nanosheets for enhanced visible-light-driven water oxidation, Appl. Catal. B, Environ. 223 (2018) 2–9.
[154] B. Xue, H.-Y. Jiang, T. Sun, F. Mao, ZnS@g-C_3N_4 composite photocatalysts: in situ synthesis and enhanced visible-light photocatalytic activity, Catal. Lett. 146 (2016) 2185–2192.
[155] M. Yoon, Y. Oh, S. Hong, J.S. Lee, R. Boppella, S.H. Kim, F. Marques Mota, S.O. Kim, D.H. Kim, Synergistically enhanced photocatalytic activity of graphitic carbon nitride and WO_3 nanohybrids mediated by photo-Fenton reaction and H_2O_2, Appl. Catal. B Environ. 206 (2017) 263–270.
[156] D. Yang, H. Zou, Y. Wu, J. Shi, S. Zhang, X. Wang, P. Han, Z. Tong, Z. Jiang, Constructing quantum dots@flake graphitic carbon nitride isotype heterojunctions for enhanced visible-light-driven NADH regeneration and enzymatic hydrogenation, Ind. Eng. Chem. Res. 56 (2017) 6247–6255.
[157] X. Wang, W. Mao, J. Zhang, Y. Han, C. Quan, Q. Zhang, T. Yang, J. Yang, X. Li, W. Huang, Facile fabrication of highly efficient g-C_3N_4/$BiFeO_3$ nanocomposites with enhanced visible light photocatalytic activities, J. Colloid Interface Sci. 448 (2015) 17–23.
[158] Y. Cheng, Y. Wang, Y. Zheng, Y. Qin, Two-step self-assembly of nanodisks into plate-built cylinders through oriented aggregation, J. Phys. Chem. B 109 (2005) 11548–11551.
[159] C.F. Lee, Interface stability, interface fluctuations, and the Gibbs-Thomson relationship in motility-induced phase separations, Soft Matter 13 (2017) 376–385.
[160] D. Zeng, W. Xu, W. Ong, J. Xu, H. Ren, Y. Chen, Toward noble-metal-free visible-light-driven photocatalytic hydrogen evolution: monodisperse sub-15 nm Ni_2P nanoparticles anchored on porous g-C_3N_4 nanosheets to engineer 0D-2D heterojunction interfaces, Appl. Catal. B Environ. 221 (2018) 47–55.
[161] Y. Li, Y. Xue, J. Tian, X. Song, X. Zhang, X. Wang, H. Cui, Silver oxide decorated graphitic carbon nitride for the realization of photocatalytic degradation over the full solar spectrum: from UV to NIR region, Sol. Energy Mater. Sol. Cells 168 (2017) 100–111.
[162] Q. Li, Y. Cao, C. Li, L. Zong, X. Wang, J. Yang, Preparation of Ag_3PO_4-loaded carbon nitride nanosheets and investigation of their visible light photocatalytic activity, J. Appl. Stat. 6 (2014) 2153–2158.
[163] X. Yang, Z. Chen, J. Xu, H. Tang, K. Chen, Y. Jiang, Tuning the morphology of g-C_3N_4 for improvement of Z-scheme photocatalytic water oxidation, Appl. Mater. Interfaces 7 (2015) 15285–15293.
[164] B. Jia, W. Zhao, L. Fan, G. Yin, Y. Cheng, F. Huang, Silver cyanamide nanoparticles decorated ultrathin graphitic carbon nitride nanosheets for enhanced visible-light-driven photocatalysis, Catal. Sci. Technol. 8 (2018) 1447–1453.
[165] R. Wang, X. Kong, W. Zhang, W. Zhu, L. Huang, J. Wang, X. Zhang, X. Liu, N. Hu, Y. Suo, J. Wang, Mechanism insight into rapid photocatalytic disinfection of Salmonella based on vanadate QDs-interspersed g-C_3N_4 heterostructures, Appl. Catal. B Environ. 225 (2018) 228–237.
[166] H. Yu, P. Xiao, P. Wang, J. Yu, Amorphous molybdenum sulfide as highly efficient electron-cocatalyst for enhanced photocatalytic H_2 evolution, Applied Catal. B, Environ. 193 (2016) 217–225.
[167] T. Wu, P. Wang, J. Qian, Y. Ao, C. Wang, J. Hou, Noble-metal-free nickel phosphide modified CdS/C_3N_4 nanorods for dramatically enhanced photocatalytic hydrogen evolution under visible light irradiation, Dalton Trans. 46 (2017) 13793–13801.
[168] P. Wang, T. Wu, C. Wang, J. Hou, J. Qian, Y. Ao, Combining heterojunction engineering with surface cocatalyst modification to synergistically enhance the photocatalytic hydrogen evolution performance of cadmium sulfide nanorods, ACS Sustain. Chem. Eng. 5 (2017) 7670–7677.
[169] Y. Zhou, G. Chen, Y. Yu, Y. Feng, Y. Zheng, F. He, Z. Han, An efficient method to enhance the stability of sulphide semiconductor photocatalysts: a case study of N-doped ZnS, Phys. Chem. Chem. Phys. 17 (2015) 1870–1876.
[170] H. Xu, L. Wu, L. Jin, K. Wu, Combination mechanism and enhanced visible-light photocatalytic activity and stability of CdS/g-C_3N_4 heterojunctions, J. Mater. Sci. Technol. 33 (2017) 30–38.
[171] W. Feng, Y. Wang, X. Huang, K. Wang, F. Gao, Y. Zhao, B. Wang, L. Zhang, P. Liu, One-pot construction of 1D/2D $Zn_{1-x}Cd_xS$/D-ZnS$(en)_{0.5}$ composites with perfect heterojunctions and their superior visible-light-driven photocatalytic H_2 evolution, Appl. Catal. B, Environ. 220 (2018) 324–336.
[172] Y. Liu, X. Zhang, J. Wang, P. Yang, In situ growth of sulfide/g-C_3N_4 nano-heterostructures with an adjusted band gap toward enhanced visible photocatalysis, Phys. Chem. Chem. Phys. 18 (2016) 31513–31520.
[173] S. Ma, Y. Song, P. Xu, X. Fu, Z. Ye, J. Xue, Facile one-step synthesis of $Cu_{1.96}S$/g-C_3N_4 0D/2D p-n heterojunctions with enhanced visible light photoactivity toward ciprofloxacin degradation, Mater. Lett. 213 (2018) 370–373.
[174] S.B. Kokane, R. Sasikala, D.M. Phase, S.D. Sartale, In_2S_3 nanoparticles dispersed on g-C_3N_4 nanosheets: role of heterojunctions in photoinduced charge transfer and photoelectrochemical and photocatalytic performance, J. Mater. Sci. 52 (2017) 7077–7090.
[175] J. Yan, H. Wu, H. Chen, Y. Zhang, F. Zhang, S. Frank, Fabrication of TiO_2/C_3N_4 heterostructure for enhanced photocatalytic Z-scheme overall water splitting, Applied Catal. B, Environ. 191 (2016) 130–137.
[176] S. Anandan, J.J. Wu, D. Bahnemann, A. Emeline, M. Ashokkumar, Crumpled Cu_2O-g-C_3N_4 nanosheets for hydrogen evolution catalysis, Colloids Surf. A Physicochem. Eng. Asp. 527 (2017) 34–41.
[177] D. Huang, C. Hu, G. Zeng, M. Cheng, P. Xu, X. Gong, R. Wang, W. Xue, Combination of Fenton processes and biotreatment for wastewater treatment and soil remediation, Sci. Total Environ. 574 (2017) 1599–1610.
[178] C. Hu, D. Huang, G. Zeng, M. Cheng, X. Gong, R. Wang, W. Xue, Z. Hu, Y. Liu, The combination of Fenton process and Phanerochaete chrysosporium for the removal of bisphenol A in river sediments: mechanism related to extracellular enzyme, organic acid and iron, Chem. Eng. J. 338 (2018) 432–439.
[179] X. Lü, J. Shen, D. Fan, J. Wang, Z. Cui, J. Xie, Solvothermal engineering of bismuth molybdate with C_3N_4 nanosheets, and enhanced photocatalytic activity, Res. Chem. Intermed. 41 (2015) 9629–9642.
[180] W. Wang, T. An, G. Li, D. Xia, H. Zhao, J.C. Yu, P.K. Wong, Earth-abundant Ni_2P/g-C_3N_4 lamellar nanohydrids for enhanced photocatalytic hydrogen evolution and bacterial inactivation under visible light irradiation, Appl. Catal. B Environ. 217 (2017) 570–580.
[181] D. Zeng, W.-J. Ong, H. Zheng, M. Wu, Y. Chen, D. Peng, M. Han, $Ni_{12}P5$ nanoparticles embedded into porous g-C_3N_4 nanosheets as a noble-metal-free heterostructure photocatalyst for efficient H_2 production under visible light, J. Mater. Chem. A 5 (2017) 16171-16178.5.
[182] M. Rakibuddin, H. Kim, M. Ehtisham, Graphite-like carbon nitride (C_3N_4) modified N-doped $LaTiO_3$ nanocomposite for higher visible light photocatalytic and photo-electrochemical performance, Appl. Surf. Sci. 452 (2018) 400–412.
[183] G. Zhou, M. Wu, Q. Xing, F. Li, H. Liu, X. Luo, J. Zou, Synthesis and characterizations of metal-free semiconductor/MOFs with good stability and high photocatalytic activity for H_2 evolution : a novel Z-scheme heterostructured photocatalyst formed by covalent bonds, Appl. Catal. B Environ. 220 (2018) 607–614.
[184] D. Yuan, J. Ding, J. Zhou, L. Wang, H. Wan, W. Dai, G. Guan, Graphite carbon nitride nanosheets decorated with ZIF-8 nanoparticles: effects of the preparation method and their special hybrid structures on the photocatalytic performance, J. Alloys Compd. 762 (2018) 98–108.
[185] G.H. Carey, A.L. Abdelhady, Z. Ning, S.M. Thon, O.M. Bakr, E.H. Sargent, Colloidal quantum dot solar cells, Chem. Rev. 115 (2015) 12732–12763.
[186] N. Shi, W. Cheng, H. Zhou, T. Fan, M. Niederberger, Facile synthesis of monodisperse Co_3O_4 quantum dots with efficient oxygen evolution activity, Chem. Commun. 51 (2015) 1338–1340.
[187] M.I. Čomor, J.M. Nedeljković, Enhanced photocorrosion stability of colloidal cadmium sulphide-silica nanocomposites, J. Mater. Sci. Lett. 18 (1999) 1583–1585.
[188] S. Yamashita, M. Hamada, S. Nakanishi, H. Saito, Y. Nosaka, S. Wakida, V. Biju, Auger ionization beats photo-oxidation of semiconductor quantum dots: extended stability of single-molecule photoluminescence, Angew. Chemie 127 (2015) 3964–3968.
[189] L. Yao, D. Wei, Y. Ni, D. Yan, C. Hu, Surface localization of CdZnS quantum dots onto 2D g-C_3N_4 ultrathin microribbons: highly efficient visible light-induced H_2-generation, Nano Energy 26 (2016) 248–256.
[190] R. Dadigala, R.K. Bandi, B.R. Gangapuram, V. Guttena, Carbon dots and Ag nanoparticles decorated g-C_3N_4 nanosheets for enhanced organic pollutants degradation under sunlight irradiation, J. Photochem. Photobiol. A Chem. 342 (2017) 42–52.

[191] Y. Deng, L. Tang, C. Feng, G. Zeng, J. Wang, Y. Lu, Y. Liu, J. Yu, S. Chen, Y. Zhou, Construction of plasmonic Ag and nitrogen-doped graphene quantum dots codecorated ultrathin graphitic carbon nitride nanosheet composites with enhanced photocatalytic activity: full-spectrum response ability and mechanism insight, ACS Appl. Mater. Interfaces 9 (2017) 42816–42828.
[192] Z. Pan, Y. Zheng, F. Guo, P. Niu, X. Wang, Decorating CoP and Pt nanoparticles on graphitic carbon nitride nanosheets to promote overall water splitting by conjugated polymers, ChemSusChem 10 (2017) 87–90.
[193] S. Zhang, J. Li, X. Wang, Y. Huang, M. Zeng, J. Xu, In situ ion exchange synthesis of strongly coupled Ag@AgCl/g-C_3N_4 porous nanosheets as plasmonic photocatalyst for highly efficient visible-light photocatalysis, ACS Appl. Mater. Interfaces 6 (2014) 22116–22125.
[194] M. Long, W. Cai, Advanced nanoarchitectures of silver/silver compound composites for photochemical reactions, Nanoscale 6 (2014) 7730–7742.
[195] X. Yao, X. Liu, X. Hu, Synthesis of the Ag/AgCl/g-C_3N_4 composite with high photocatalytic activity under visible light irradiation, ChemCatChem 6 (2014) 3409–3418.
[196] J. Li, H. Hao, J. Zhou, W. Li, N. Lei, L. Guo, Ag@AgCl QDs decorated g-C_3N_4 nanoplates: the photoinduced charge transfer behavior under visible light and full arc irradiation, Appl. Surf. Sci. 422 (2017) 626–637.
[197] Z. Jiang, K. Qian, C. Zhu, H. Sun, W. Wan, J. Xie, H. Li, P.K. Wong, S. Yuan, Carbon nitride coupled with CdS-TiO_2 nanodots as 2D/0D ternary composite with enhanced photocatalytic H_2 evolution: a novel efficient three-level electron transfer process, Appl. Catal. B Environ. 210 (2017) 194–204.
[198] Y. Gao, J. Lin, Q. Zhang, H. Yu, F. Ding, B. Xu, Y. Sun, Z. Xu, Facile synthesis of heterostructured YVO_4/g-C_3N_4/Ag photocatalysts with enhanced visible-light photocatalytic performance, Appl. Catal. B Environ. 224 (2018) 586–593.
[199] F. Chen, Q. Yang, Y. Wang, J. Zhao, D. Wang, X. Li, Z. Guo, H. Wang, Y. Deng, C. Niu, G. Zeng, Novel ternary heterojunction photcocatalyst of Ag nanoparticles and g-C_3N_4 nanosheets co-modified $BiVO_4$ for wider spectrum visible-light photocatalytic degradation of refractory pollutant, Appl. Catal. B Environ. 205 (2017) 133–147.
[200] J. Wu, X. Shen, X. Miao, Z. Ji, J. Wang, T. Wang, M. Liu, An all-solid-state Z-scheme g-C_3N_4/Ag/Ag_3VO_4 photocatalyst with enhanced visible-light photocatalytic performance, Eur. J. Inorg. Chem. 2017 (2017) 2845–2853.
[201] X. Yang, H. Tang, J. Xu, M. Antonietti, M. Shalom, Silver phosphate/graphitic carbon nitride as an efficient photocatalytic tandem system for oxygen evolution, ChemSusChem 8 (2015) 1350–1358.
[202] L. Tang, C. Feng, Y. Deng, G. Zeng, J. Wang, Y. Liu, H. Feng, J. Wang, Enhanced photocatalytic activity of ternary Ag/g-C_3N_4/$NaTaO_3$ photocatalysts under wide spectrum light radiation : the high potential band protection mechanism, Appl. Catal. B Environ. 230 (2018) 102–114.
[203] L. Shi, Z. Li, K. Marcus, G. Wang, K. Liang, W. Niu, Y. Yang, Integration of Au nanoparticles with a g-C_3N_4 based heterostructure: switching charge transfer from type-II to Z-scheme for enhanced visible light photocatalysis, Chem. Commun. 54 (2018) 3747–3750.
[204] H. He, L. Huang, Z. Zhong, S. Tan, Constructing three-dimensional porous graphene-carbon quantum dots/g-C_3N_4 nanosheet aerogel metal-free photocatalyst with enhanced photocatalytic activity, Appl. Surf. Sci. 441 (2018) 285–294.
[205] X. Miao, Z. Ji, J. Wu, X. Shen, J. Wang, L. Kong, M. Liu, g-C_3N_4/AgBr nanocomposite decorated with carbon dots as a highly efficient visible-light-driven photocatalyst, J. Colloid Interface Sci. 502 (2017) 24–32.
[206] J. Xiao, Q. Han, Y. Xie, J. Yang, Q. Su, Y. Chen, H. Cao, Is C_3N_4 chemically stable toward reactive oxygen species in sunlight-driven water treatment? Environ. Sci. Technol. 51 (2017) 13380–13387.
[207] Z. Chen, E. Vorobyeva, S. Mitchell, E. Fako, M.A. Ortuño, N. López, S.M. Collins, P.A. Midgley, S. Richard, G. Vilé, J. Pérez-ramírez, A heterogeneous single-atom palladium catalyst surpassing homogeneous systems for Suzuki coupling, Nature Nanotech. (2018).
[208] G. Gao, Y. Jiao, E.R. Waclawik, A. Du, Single atom (Pd/Pt) supported on graphitic carbon nitride as an efficient photocatalyst for visible-light reduction of carbon dioxide, J. Am. Chem. Soc. 138 (2016) 6292–6297.
[209] X. Li, W. Bi, L. Zhang, S. Tao, W. Chu, Q. Zhang, Y. Luo, C. Wu, Y. Xie, Single-atom Pt as co-catalyst for enhanced photocatalytic H_2 evolution, Adv. Mater. 28 (2016) 2427–2431.
[210] L. Tian, X. Yang, Q. Liu, F. Qu, H. Tang, Anchoring metal-organic framework nanoparticles on graphitic carbon nitrides for solar-driven photocatalytic hydrogen evolution, Appl. Surf. Sci. 455 (2018) 403–409.
[211] H. Wang, X. Yuan, Y. Wu, G. Zeng, X. Chen, L. Leng, H. Li, Synthesis and applications of novel graphitic carbon nitride/metal-organic frameworks mesoporous photocatalyst for dyes removal, Appl. Catal. B, Environ. 174-175 (2015) 445–454.
[212] X. Gong, D. Huang, Y. Liu, G. Zeng, R. Wang, J. Wei, C. Huang, P. Xu, J. Wan, C. Zhang, Pyrolysis and reutilization of plant residues after phytoremediation of heavy metals contaminated sediments: for heavy metals stabilization and dye adsorption, Bioresour. Technol. 253 (2018) 64–71.
[213] D. Huang, L. Liu, G. Zeng, P. Xu, C. Huang, L. Deng, R. Wang, J. Wan, The effects of rice straw biochar on indigenous microbial community and enzymes activity in heavy metal-contaminated sediment, Chemosphere 174 (2017) 545–553.
[214] D. Huang, X. Gong, Y. Liu, G. Zeng, C. Lai, H. Bashir, L. Zhou, D. Wang, P. Xu, M. Cheng, J. Wan, Effects of calcium at toxic concentrations of cadmium in plants, Planta 245 (2017) 863–873.
[215] W. Xue, D. Huang, G. Zeng, J. Wan, C. Zhang, R. Xu, M. Cheng, R. Deng, Nanoscale zero-valent iron coated with rhamnolipid as an effective stabilizer for immobilization of Cd and Pb in river sediments, J. Hazard. Mater. 341 (2018) 381–389.
[216] D. Huang, R. Deng, J. Wan, G. Zeng, W. Xue, X. Wen, C. Zhou, L. Hu, X. Liu, X. Guo, X. Ren, Remediation of lead-contaminated sediment by biochar-supported nano-chlorapatite: accompanied with the change of available phosphorus and organic matters, J. Hazard. Mater. 348 (2018) 109–116.
[217] G. Jiang, X. Li, M. Lan, T. Shen, X. Lv, F. Dong, S. Zhang, Monodisperse bismuth nanoparticles decorated graphitic carbon nitride: enhanced visible-light-response photocatalytic NO removal and reaction pathway, Appl. Catal. B Environ. 205 (2017) 532–540.
[218] Z. Liang, Q. Wen, X. Wang, F. Zhang, Y. Yu, Chemically stable and reusable nano zero-valent iron/graphite-like carbon nitride nanohybrid for efficient photocatalytic treatment of Cr (VI) and rhodamine B under visible light, Appl. Surf. Sci. 386 (2016) 451–459.
[219] X. Gong, D. Huang, Y. Liu, G. Zeng, R. Wang, J. Wan, C. Zhang, M. Cheng, X. Qin, W. Xue, Stabilized nanoscale zerovalent iron mediated cadmium accumulation and oxidative damage of Boehmeria nivea (L.) Gaudich cultivated in cadmium contaminated sediments, Environ. Sci. Technol. 51 (2017) 11308–11316.
[220] D. Huang, W. Xue, G. Zeng, J. Wan, G. Chen, C. Huang, C. Zhang, M. Cheng, P. Xu, Immobilization of Cd in river sediments by sodium alginate modified nanoscale zero-valent iron: impact on enzyme activities and microbial community diversity, Water Res. 106 (2016) 15–25.
[221] D. Huang, Z. Hu, Z. Peng, G. Zeng, G. Chen, C. Zhang, M. Cheng, J. Wan, X. Wang, X. Qin, Cadmium immobilization in river sediment using stabilized nanoscale zero-valent iron with enhanced transport by polysaccharide coating, J. Environ. Manag. 210 (2018) 191–200.
[222] D. Huang, X. Qin, Z. Peng, Y. Liu, X. Gong, G. Zeng, C. Huang, M. Cheng, W. Xue, X. Wang, Z. Hu, Nanoscale zero-valent iron assisted phytoremediation of Pb in sediment: impacts on metal accumulation and antioxidative system of Lolium perenne, Ecotox. Environ. Saf. 153 (2018) 229–237.